

The Koala: A Fast Blue Optical Transient with Luminous Radio Emission from a Starburst Dwarf Galaxy at $z = 0.27$

ANNA Y. Q. HO,¹ DANIEL A. PERLEY,² S. R. KULKARNI,¹ IGOR ANDREONI,¹ ERIC C. BELLM,³ KEVIN B. BURDGE,¹
POONAM CHANDRA,⁴ MICHAEL COUGHLIN,⁵ KISHALAY DE,¹ DILLON Z. J. DONG,¹ V. ZACH GOLKHOV,^{3,6}
MATTHEW J. GRAHAM,¹ DMITRY D. FREDERIKS,⁷ GEORGE HELOU,⁸ ASSAF HORESH,⁹ RUSS R. LAHER,⁸ FRANK J. MASCI,⁸
ANNA RIDNAIA,⁷ BEN RUSHOLME,⁸ DAVID L. SHUPE,⁸ AND DMITRY S. SVINKIN⁷

¹*Cahill Center for Astrophysics, California Institute of Technology, MC 249-17, 1200 E California Boulevard, Pasadena, CA, 91125, USA*

²*Astrophysics Research Institute, Liverpool John Moores University, IC2, Liverpool Science Park, 146 Brownlow Hill, Liverpool L3 5RF, UK*

³*DIRAC Institute, Department of Astronomy, University of Washington, 3910 15th Avenue NE, Seattle, WA 98195, USA*

⁴*National Centre for Radio Astrophysics, Tata Institute of Fundamental Research, PO Box 3, Pune, 411007, India*

⁵*School of Physics and Astronomy, University of Minnesota, Minneapolis, Minnesota 55455, USA*

⁶*The eScience Institute, University of Washington, Seattle, WA 98195, USA**

⁷*Ioffe Institute, Politekhnikeskaya 26, St. Petersburg 194021, Russia*

⁸*IPAC, California Institute of Technology, 1200 E. California Blvd, Pasadena, CA 91125, USA*

⁹*Racah Institute of Physics, The Hebrew University of Jerusalem, Jerusalem 91904, Israel*

Submitted to The Astrophysical Journal

Abstract

We present ZTF18abvkwla (the “Koala”), a fast blue optical transient discovered in the Zwicky Transient Facility (ZTF) One-Day Cadence (1DC) Survey. This event has a number of features in common with the groundbreaking transient AT2018cow: blue colors at peak ($g - r \approx -0.5$), a short rise time from half-max of under two days, a decay time of only three days, a high optical luminosity ($M_{g,\text{peak}} \approx -20.8$), a hot ($\geq 40,000$ K) featureless spectrum at peak light, and a luminous radio counterpart ($\nu L_\nu \geq 10^{40}$ erg s⁻¹ at 10 GHz). The radio luminosity of ZTF18abvkwla exceeds that of AT2018cow by an order of magnitude, and the late-time ($\Delta t \geq 80$ d) light curve resembles that of long-duration gamma-ray bursts (GRBs). The host galaxy is a dwarf starburst galaxy ($M \approx 5 \times 10^8 M_\odot$, $\text{SFR} \approx 7 M_\odot \text{yr}^{-1}$) that is moderately metal-enriched ($\log [\text{O}/\text{H}] \approx 8.5$), similar to the hosts of GRBs and superluminous supernovae. As in AT2018cow, the radio and optical emission in ZTF18abvkwla likely arise from two separate components: the radio from fast-moving collimated ejecta and the optical from shock-interaction with confined dense material ($< 0.07 M_\odot$ in $\sim 10^{15}$ cm). Compiling transients in the literature with $t_{\text{rise}} < 5$ d and $M_{\text{peak}} < -20$, we find that a significant number are engine-powered, and suggest that the high peak optical luminosity is directly related to the presence of this engine. From 18 months of the 1DC survey, we find that transients in this rise-luminosity phase space are at least two orders of magnitude less common than CCSNe. Finally, we discuss strategies for identifying such events with future facilities like the Large Synoptic Survey Telescope, and prospects for detecting accompanying X-ray and radio emission.

1. INTRODUCTION

Historically, the cadence of optical time-domain surveys was tuned to detecting Type Ia supernovae (SNe),

whose optical light curves rise from first light to peak in 15–20 days (Miller et al. 2020). Recognizing that this observing strategy resulted in “gaps” in timescale-luminosity phase-space, surveys such as the Palomar Transient Factory (Law et al. 2009; Rau et al. 2009) and the Pan-STARRS1 Medium Deep Survey (Drout et al. 2014) sought to systematically chart the landscape of short-timescale (< 10 day) phenomena. These efforts delineated populations of fast transients spanning

Corresponding author: Anna Y. Q. Ho
ah@astro.caltech.edu

* Moore-Sloan, WRF Innovation in Data Science, and DIRAC Fellow

many orders of magnitude in peak luminosity, from faint calcium-rich transients (Kasliwal et al. 2012) to luminous relativistic explosions (Cenko et al. 2013).

A population of particular recent interest is “fast evolving luminous transients” (Rest et al. 2018) or “fast blue optical transients” (Margutti et al. 2019). A consistent definition of this “class” does not yet exist; these terms typically refer to a rise time and peak luminosity too fast and too luminous, respectively, to be explained by the radioactive decay of ^{56}Ni . Although they likely arise from a variety of progenitors, fast-luminous transients are primarily found in star-forming galaxies (Drout et al. 2014; Pursiainen et al. 2018) and therefore are thought to represent a variety of poorly understood endpoints of massive-star evolution. As summarized in Kasen (2017), a possible power mechanism is shock breakout or shock-cooling emission from material that is closely confined to the progenitor star at the time of explosion; this is of interest because late-stage eruptive mass-loss in massive stars is known to be important yet poorly understood (Smith 2014). Another possibility, also reviewed in Kasen (2017), is a central engine such as a newborn magnetar or accreting black hole.

Most fast-luminous optical transients have been found in archival searches of optical-survey data, including PS1 (Drout et al. 2014), the Dark Energy Survey (Pursiainen et al. 2018), Kepler (Rest et al. 2018), and the Supernova Legacy Survey (Arcavi et al. 2016). A handful have been discovered while the transient was still active, enabling prompt follow-up observations. For example, spectroscopic monitoring of the fast-rising transient iPTF16asu revealed that as the optical light curve declined, the spectrum developed features typical of a broad-lined Ic SN (Whitesides et al. 2017; Wang et al. 2019). The same behavior was observed in ZTF18abukavn (SN 2018gep; Ho et al. 2019b). Unlike most Ic-BL SNe, the peak of the optical light curve of iPTF16asu and SN 2018gep was not powered by the radioactive decay of ^{56}Ni . This fast and luminous component could be related to the activity of a jet (Nakar 2015), although no radio emission was detected in either SN that would confirm the presence of a relativistic outflow (Whitesides et al. 2017; Ho et al. 2019b). Regardless of whether there was a jet, the early optical emission likely arose from interaction with material ejected shortly prior to core-collapse (Ho et al. 2019b).

The discovery of the fast-luminous transient AT2018cow (Prentice et al. 2018) generated considerable excitement because of its proximity ($z = 0.0141$) and therefore the opportunity for detailed observations. AT2018cow had several remarkable features: (1) near-relativistic ejecta velocities at early times, from optical

spectroscopy (Perley et al. 2019a); (2) luminous and fast-varying X-ray emission suggesting an exposed central engine (Rivera Sandoval et al. 2018; Ho et al. 2019a; Margutti et al. 2019); (3) high-velocity emission lines of hydrogen and helium emerging at late times (Perley et al. 2019a); (4) no second peak that would indicate a significant role for radioactive ejecta in powering the light curve (Perley et al. 2019a); and (5) luminous sub-millimeter emission indicating a large explosion energy injected into a shell of very dense material (Ho et al. 2019a; Huang et al. 2019). Despite extensive observations across the electromagnetic spectrum, the progenitor of AT2018cow is unknown. One suggestion is a massive-star explosion that resulted in the formation of an accreting black hole or magnetar, that drove a mildly relativistic jet or wind (Perley et al. 2019a; Margutti et al. 2019; Ho et al. 2019a). Other suggestions include an electron-capture SN (Lyutikov, & Toonen 2019) and a tidal disruption event (TDE; Vinkó et al. 2015; Perley et al. 2019a; Kuin et al. 2019). Fox & Smith (2019) pointed out the similarity between AT2018cow and interaction-powered Type Ibn SNe; indeed, if AT2018cow had a massive-star progenitor, the presence of dense confined CSM also points to eruptive mass-loss shortly before core-collapse.

Here we report the discovery in Zwicky Transient Facility (ZTF) data of ZTF18abvkwla¹, a fast-rising luminous optical transient at $z = 0.27$. In Section 2 we present the key observational features of ZTF18abvkwla—a rest-frame g -band light curve similar to that of AT2018cow, a luminous radio counterpart similar to gamma-ray burst (GRB) afterglows, a starburst dwarf host galaxy—and in Section 3 we draw comparisons to transients in the literature. For a comparison sample, we choose transients with $t_{\text{rise}} < 5$ d and $M < -20$, where t_{rise} is defined from 0.75 mag below peak to peak (half-max to max in flux space). We use a cut of $M < -20$ to exclude “normal” Type Ibn SNe (Hosseinzadeh et al. 2017) and we exclude the hundreds of optical afterglows discovered in GRB follow-up observations (Kann et al. 2010). The comparison sample is shown in Table 1 and Figure 1.

In Section 4.1 we suggest that the optical emission from ZTF18abvkwla is thermal emission from shock breakout in dense confined material. Note that most transients in Table 1 have similarly blue colors and featureless thermal spectra at peak, unlike GRB afterglows which arise from synchrotron radiation. In Section 4.2 we suggest that as in AT2018cow, the radio emission

¹ nicknamed “Koala” on account of the last four letters of its ZTF ID

Table 1. Transients in the literature with $t_{\text{rise}} < 5$ d and $M < -20$. Timescales are presented in rest-frame and measured using the light curve that most closely matches rest-frame g . Luminosity is corrected for Galactic extinction, assuming zero host-galaxy extinction in all cases except for iPTF15ul and SN 2011kl.

Name	Redshift	$M_{g,\text{max}}$	t_{rise} days	t_{fade} days	Ref
Dougie	0.19	-23.03 ± 0.13	3.92 ± 0.14	9.69 ± 1.19	[1]
SN 2011kl	0.677	-20.31 ± 0.13	4.97 ± 1.20	17.70 ± 5.82	[2,3]
SNLS04D4ec	0.593	-20.26 ± 0.03	< 3.81	8.60 ± 0.43	[4]
SNLS05D2bk	0.699	-20.39 ± 0.02	2.90 ± 0.06	12.75 ± 0.78	[4]
SNLS06D1hc	0.555	-20.28 ± 0.03	4.59 ± 0.06	12.35 ± 0.45	[4]
iPTF15ul	0.066	-21.2 ± 0.3	1.53 ± 0.05	3.72 ± 0.08	[5]
DES16X1eho	0.76	-20.39 ± 0.09	$1.28\text{--}2.53$	1.01 ± 0.27	[6]
iPTF16asu	0.187	-20.3 ± 0.1	1.14 ± 0.13	10.62 ± 0.55	[7]
AT2018scow	0.0141	-20.89 ± 0.06	1.43 ± 0.08	1.95 ± 0.06	[8,9]

References— [1] Vinkó et al. (2015), [2] Greiner et al. (2015), [3] Kann et al. (2019), [4] Arcavi et al. (2016), [5] Hosseinzadeh et al. (2017), [6] Pursiainen et al. (2018) [7] Whitesides et al. (2017), [8] Prentice et al. (2018) [9] Perley et al. (2019a)

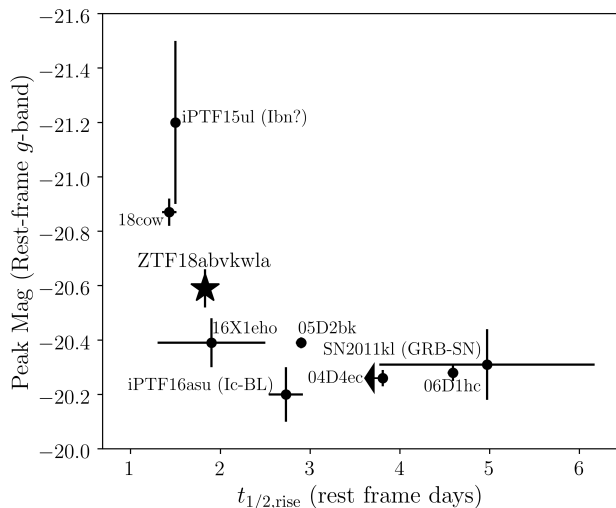


Figure 1. Phase-space of luminosity and rise time considered in this paper. Data taken from Hosseinzadeh et al. (2017); Whitesides et al. (2017); Pursiainen et al. (2018); Perley et al. (2019a). We do not show the transient Dougie (Vinkó et al. 2015), which had a peak absolute magnitude of -23 . Note that iPTF15ul has a large host-galaxy extinction correction, whereas the other sources have zero host extinction correction.

from ZTF18abvkwla arises from a separate component from the optical emission, with sustained fast velocities ($v \gtrsim 0.5c$) one year after explosion. Given the likely presence of a central engine in ZTF18abvkwla, AT2018scow, and several other transients in Table 1, we conclude that a high peak luminosity is directly related to the activity of this engine. Finally, in Section 5 we use

18 months of survey observations to estimate the rate of transients in the phase-space of Figure 1, and find that the rate is 2–3 times smaller than the CC SN rate.

Throughout this paper, we use a standard Λ CDM cosmology (Planck Collaboration et al. 2016) and times are reported in UT. Optical magnitudes are reported in the AB system (Oke, & Gunn 1983), and corrected for foreground Galactic extinction using reddening measurements in Schlafly & Finkbeiner (2011) and the extinction law from Fitzpatrick (1999).

2. DISCOVERY AND BASIC ANALYSIS

2.1. Optical

2.1.1. Photometry

Since April 2018, ZTF (Bellm et al. 2019a; Graham et al. 2019) has been conducting a wide-area ($2000\text{--}3000 \text{ deg}^2$) one-day cadence (1DC) survey in g and r (Bellm et al. 2019). The sky coverage of the 1DC survey is shown in Figure 2 and a histogram of the typical time between exposures is shown in Figure 3.

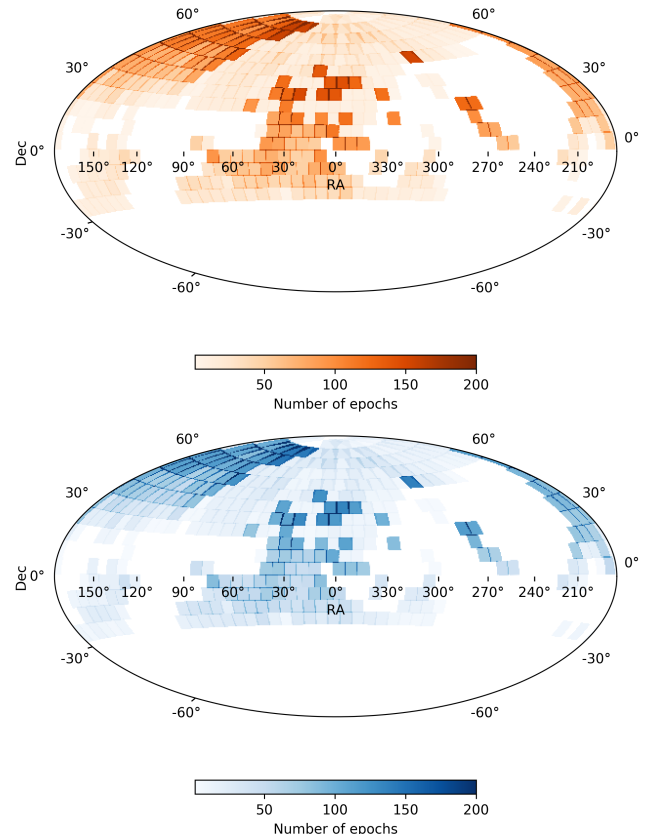


Figure 2. Number of epochs obtained by the ZTF one-day cadence survey from 3 April 2018 to 18 October 2019

The IPAC ZTF pipeline (Masci et al. 2019) uses the method described in Zackay et al. (2016) to generate

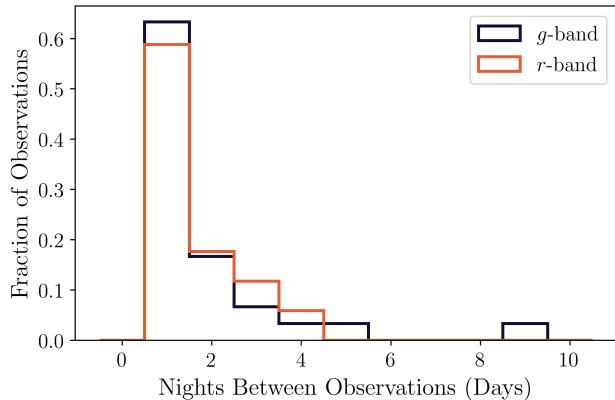


Figure 3. Histogram of times between successive observations of a field in the same filter for the ZTF one-day cadence survey. Intervals greater than 10 days are not shown.

difference images using a coadded reference image. Every $5\text{-}\sigma$ point-source detection is assigned a score based on a machine learning real-bogus metric (Mahabal et al. 2019; Duev et al. 2019), and is cross-matched against external catalogs to search for resolved and extended counterparts (Tachibana & Miller 2018). Alerts are distributed in Avro format (Patterson et al. 2019) and are filtered by the ZTF collaboration using a web-based system called the GROWTH Marshal (Kasliwal et al. 2019).

ZTF18abvkwla was discovered in an image obtained on 12 Sept 2018. The alert passed a filter designed to look for rapidly-evolving transients, and as a result we obtained a follow-up spectrum 24 hours later (Section 2.1.2). The discovery magnitude was $g = 19.73 \pm 0.16$ mag and the last non-detection was one day prior, with a limiting magnitude $g > 20.74$.

The source position was measured to be $\alpha = 02^{\text{h}}00^{\text{m}}15.19^{\text{s}}$, $\delta = +16^{\text{d}}47^{\text{m}}57.3^{\text{s}}$ (J2000), which is $0.28 \pm 0.13''$ from the nucleus of a blue ($g - r = 0.32$) extended source that has a photometric redshift of 0.11 (68 percentile confidence interval 0.08–0.29) in the eighth data release of LegacySurvey (DR8; Dey et al. 2019). At $z = 0.2714$ (Section 2.1.2) this offset corresponds to 1.9 ± 0.9 kpc. The host is approximately $2''$ (14 kpc) across.

The light curve (Figure 4; Table 2) has a similar timescale and peak luminosity to that of AT2018cow. In rest-frame g -band, the rise time is 1.83 ± 0.05 d, the fade time is 3.12 ± 0.22 d, and the peak magnitude is -20.59 ± 1.83 .

We estimate that the onset of the optical emission was around the time of the last non-detection ($t_0 = 2458372.9206$ JD) and use this as a reference epoch for the remainder of the paper.

Table 2. Optical photometry for ZTF18abvkwla from forced photometry on P48 images (Yao et al. 2019). Values have not been corrected for Galactic extinction. Phase Δt is defined from t_0 , the last non-detection.

Date (MJD)	Δt	Filter	AB Mag
58372.389800	-1.02	<i>r</i>	< 21.39
58372.420600	-0.99	<i>g</i>	< 21.56
58373.407523	0.00	<i>g</i>	19.71 ± 0.05
58373.447708	0.04	<i>r</i>	20.18 ± 0.09
58374.391343	0.98	<i>r</i>	20.00 ± 0.07
58374.406007	1.00	<i>g</i>	19.53 ± 0.05
58375.371227	1.96	<i>r</i>	19.92 ± 0.07
58375.372141	1.96	<i>r</i>	20.02 ± 0.07
58375.432708	2.03	<i>g</i>	19.65 ± 0.04
58375.433623	2.03	<i>g</i>	19.72 ± 0.05
58376.419340	3.01	<i>r</i>	20.15 ± 0.07
58376.443044	3.04	<i>g</i>	19.77 ± 0.05
58377.388819	3.98	<i>g</i>	20.10 ± 0.07
58377.426076	4.02	<i>r</i>	20.29 ± 0.09
58378.401354	4.99	<i>r</i>	20.50 ± 0.10
58378.402269	4.99	<i>r</i>	20.62 ± 0.12
58378.451944	5.04	<i>g</i>	20.64 ± 0.10
58378.452859	5.05	<i>g</i>	20.42 ± 0.09
58379.423206	6.02	<i>r</i>	20.85 ± 0.15
58379.444016	6.04	<i>g</i>	20.72 ± 0.12
58380.434988	7.03	<i>r</i>	21.04 ± 0.15
58382.338264	8.93	<i>r</i>	21.06 ± 0.27
58382.339178	8.93	<i>r</i>	21.22 ± 0.28
58382.433183	9.03	<i>g</i>	21.35 ± 0.19
58382.434155	9.03	<i>g</i>	21.56 ± 0.23
58383.479028	10.07	<i>g</i>	21.51 ± 0.21

2.1.2. Spectroscopy and Host Galaxy Properties

One day after discovery, we obtained a spectrum of ZTF18abvkwla using the Double Beam Spectrograph (DBSP; Oke & Gunn 1982) on the 200-inch Hale telescope at Palomar Observatory. We used the D55 dichroic, a slit width of 1.5 arcseconds, the 600/4000 blue grating, and the 316/7500 red grating. The spectrum was reduced using a PyRAF-based pipeline (Bellm & Sesar 2016). As shown in Figure 5, the spectrum shows a hot blue continuum with no broad features in emission or absorption. Superimposed on the spectrum are a variety of narrow emission lines typical of a star-forming galaxy ($\text{H}\alpha$, $\text{H}\beta$, $[\text{OIII}]$, $[\text{SII}]$, $[\text{OII}]$) at a redshift of $z = 0.2714$ plus the Mg II UV doublet in absorption at consistent redshift.

A blackbody fit to the continuum (after subtracting a host-galaxy continuum model, discussed later in this section) indicates an effective temperature $T \gtrsim 40,000\text{K}$, although we caution that this is a lower limit as the bulk of the energy was clearly emitted in the UV ($< 2750 \text{ \AA}$ in the rest frame) and we have no firm constraint

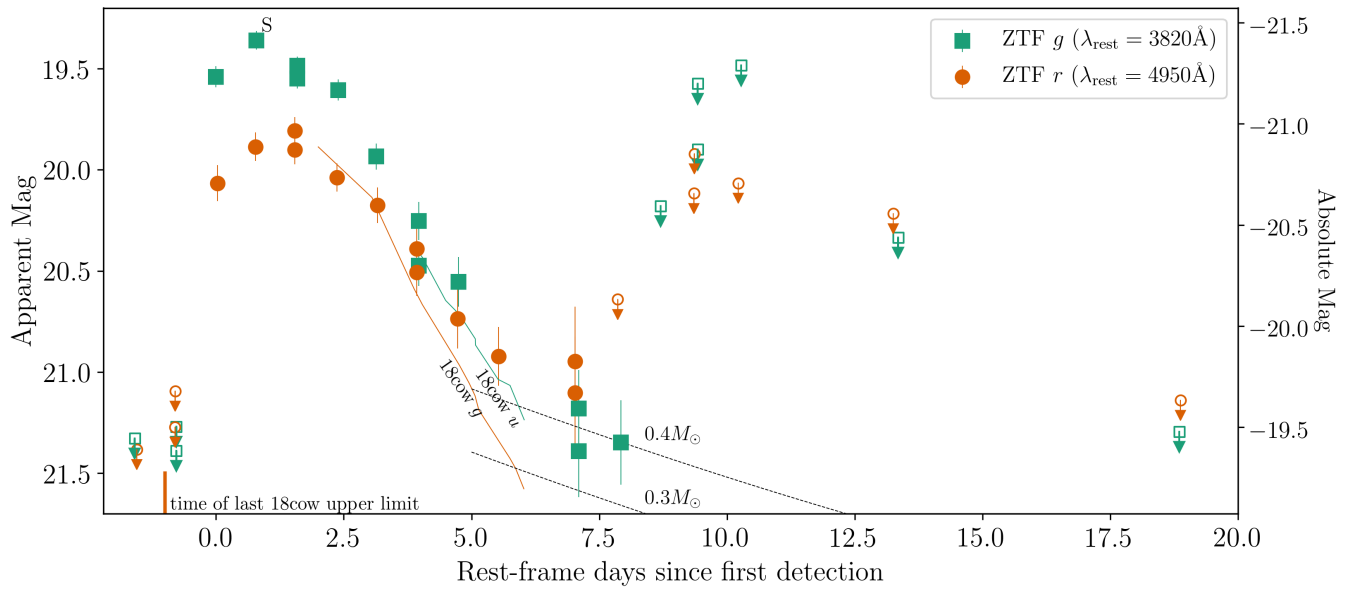


Figure 4. Light curve of ZTF18abvkwla in P48 g (filled green squares) and r (open orange circles). Inset shows magnitudes corrected for Galactic extinction, and a comparison to AT2018cow at similar rest wavelengths. The ‘S’ at the top of the inset indicates the epoch of our DBSP spectrum. Dashed lines show ^{56}Ni -powered light curves for two different nickel masses.

on the host-galaxy extinction. Together with the peak absolute magnitude of the g -band light curve, we derive a bolometric luminosity of $L_{\text{bol}} > 10^{44} \text{ erg s}^{-1}$. Assuming $T = 40,000 \text{ K}$, the photospheric radius is $R > 2 \times 10^{14} \text{ cm}$. Since the peak is 2 d after first light, the photospheric velocity is $v > 0.04c$.

On 4 Jan 2019 (+115 d), we obtained a spectrum of the host galaxy of ZTF18abvkwla using the Low Resolution Imaging Spectrometer (Oke et al. 1995) on the Keck I 10-m telescope, with the 400/3400 grism in the blue camera and the 400/8500 grating in the red camera. Exposure times were 940 and 900 seconds for the blue and red camera respectively. The spectrum was reduced and extracted using `Lpipe` (Perley 2019). The absolute calibration was established independently for each camera (red vs. blue) by calculating synthetic photometry of the output spectra in the blue and red cameras in the g and r bands, respectively, and rescaling to match the g and r photometry from SDSS DR14 (Abolfathi et al. 2018).

The host-galaxy spectrum (Figure 6) consists of a weak continuum and a series of very strong emission lines. Line fluxes were extracted using an identical procedure as in Perley et al. (2016). We first fit a model to the spectral energy distribution (SED). We used a custom IDL routine based on the templates of Bruzual & Charlot (2003) to fit the SDSS $ugriz$ photometry, including the contribution of nebular lines. As only SDSS $ugriz$ photometry is available to fit the host-galaxy SED it is difficult to constrain the nature of the stellar population of the host galaxy in detail, and we were only able to fit the simplest possible model (a continuous star-formation history). However, the stellar mass is unambiguously low ($\sim 5 \times 10^8 M_{\odot}$, comparable to the SMC),

This model was then used to produce a synthetic galaxy continuum spectrum, which was subtracted from the observed one (this correction is significant only for higher-order Balmer lines, which overlay strong galaxy absorption features). Emission line fluxes were then measured by fitting a Gaussian function to each emission line (plus a linear baseline to fit any continuum residuals). Lines that were blended or very nearby were fit in groups, and lines whose ratios are fixed from theory were tied together in fitting. A list of all measured line fluxes is given in Table 3.

The SED fitting and the emission-line analysis produce consistent estimates of $7 M_{\odot} \text{ yr}^{-1}$ for the star-formation rate, and a very high specific star-formation rate of $\sim 10^{-8} \text{ yr}^{-1}$. This implies a stellar population dominated by young stars formed in a recent triggered star-formation burst episode.

Table 3. Host emission line fluxes and equivalent widths

Species	Wavelength	Flux	Eq. Width
	(\AA)	($\text{erg cm}^{-2}\text{s}^{-1}$)	(\AA)
H α	6562.82	214.74 ± 2.71	205.9 ± 7.0
H β	4861.33	57.57 ± 1.07	41.3 ± 1.1
H γ	4340.47	26.98 ± 1.03	17.6 ± 0.8
H δ	4101.74	13.92 ± 0.91	7.2 ± 0.5
H ϵ	3970.08	11.44 ± 0.86	5.9 ± 0.4
H ζ	3889.06	9.72 ± 0.88	5.0 ± 0.5
[O II]	3727	159.44 ± 1.72	89.0 ± 2.4
[Ne III]	3868.76	16.00 ± 0.94	8.3 ± 0.5
[O III]	4363.21	<3.31	<2.1
[O III]	4958.91	66.35 ± 1.37	47.6 ± 1.4
[O III]	5006.84	196.88 ± 1.60	141.3 ± 3.1
He I	5875.62	6.76 ± 0.72	5.7 ± 0.6
[N II]	6548.06	4.90 ± 0.69	4.7 ± 0.7
[N II]	6583.57	13.91 ± 0.82	13.3 ± 0.9
[S II]	6716.44	27.86 ± 0.95	29.3 ± 1.2
[S II]	6730.82	21.81 ± 0.71	22.9 ± 0.9
O I	6300.30	6.76 ± 0.71	7.2 ± 0.8
[Ar III]	7135.79	5.49 ± 0.53	6.8 ± 0.7

We used the host galaxy spectrum (Figure 6) to calculate standard emission-line diagnostics, including metallicity estimates on a variety of scales using the Monte-Carlo code of Bianco et al. (2016). These metallicity measurements are provided in Table 4. The basic properties of the host galaxy are listed in Table 5.

2.2. Radio Observations

We obtained four epochs of observations of ZTF18abvkwla using the Karl G. Jansky Very Large Array (VLA; Perley et al. 2011) under the program VLA/18B-242 (PI: D. Perley), listed in Table 6. The first epoch was at $\Delta t \approx 81 \text{ d}$ at X-band, while the VLA was in C configuration. We used 3C138 as our flux density and bandpass calibrator, and J0204+1514 as our complex gain calibrator. The next three epochs were at $\Delta t \approx 310 \text{ d}$, $\Delta t \approx 350 \text{ d}$, and $\Delta t \approx 400 \text{ d}$, all while the VLA was in A configuration. We continued to use 3C138 but switched to J0238+1636 as our complex gain calibrator. For each observation, we ran the standard VLA calibration pipeline available in the Common Astronomy Software Applications (CASA; McMullin et al. 2007). After calibration, we inspected the data manually for further flagging. We imaged the data using the CLEAN algorithm (Högbom 1974) available in CASA, using a cell size that was 1/5 of the synthesized beamwidth. The field size was set to be the smallest magic number (10×2^n) larger than the number of cells needed to cover the primary beam.

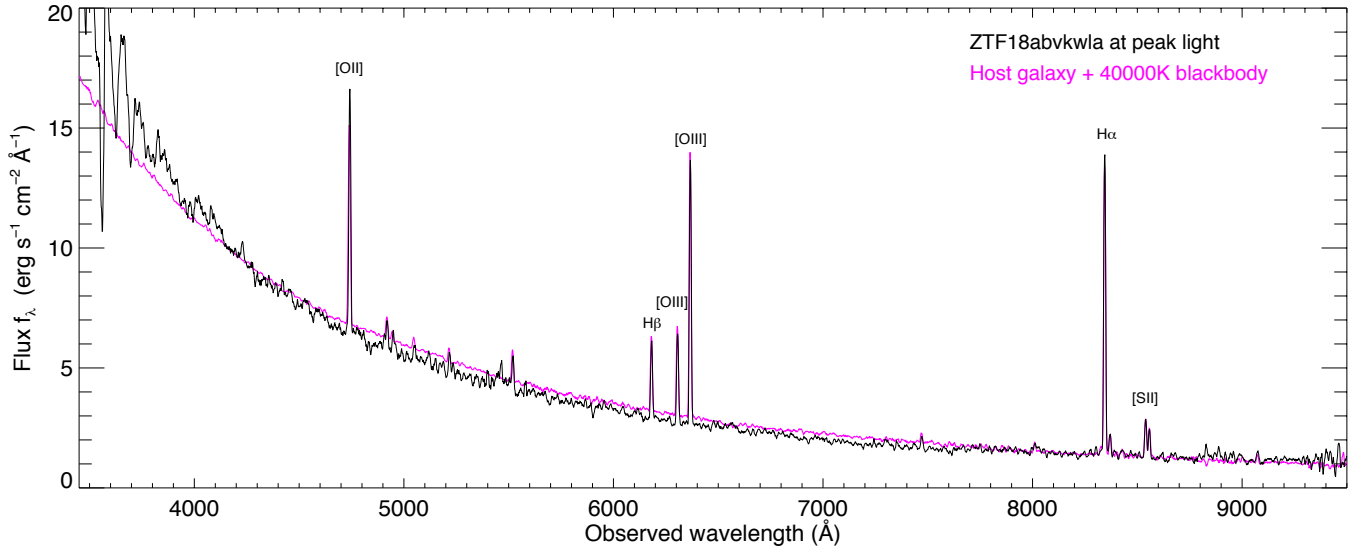


Figure 5. The spectrum of ZTF18abvkwla at the peak of the g -band optical light curve (black), which was 1 day after the first detection. The source is extremely hot and blue with no spectral features except those associated with the host galaxy. Overplotted in pink is a rescaled late-time spectrum of the host galaxy with a 40,000 K blackbody added.

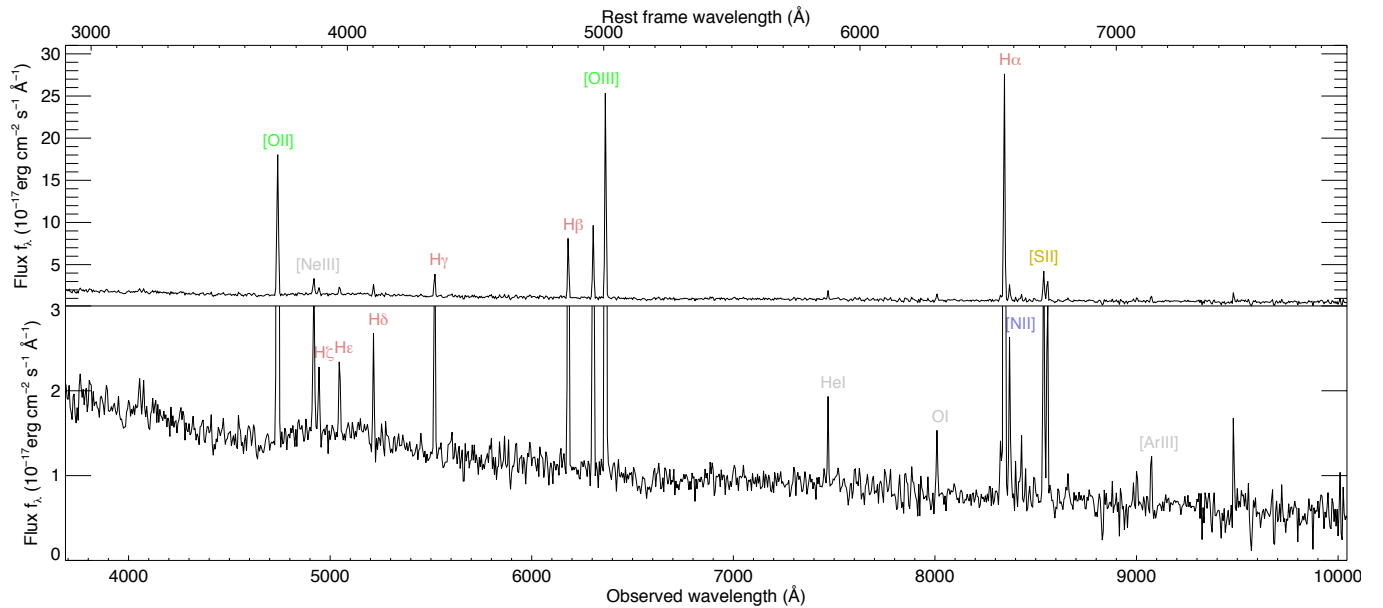


Figure 6. Spectrum of the host galaxy of ZTF18abvkwla. The scale on the bottom half has been zoomed in to show the galaxy continuum and weak emission lines.

We also obtained one epoch of observations with the upgraded Giant Metrewave Radio Telescope (GMRT; Gupta et al. 2017; Swarup et al. 1991) under a proposal for Director’s Discretionary Time (Proposal # ddtC086; PI: A. Ho). For our GMRT observations, we used 3C147 and 3C48 as our flux density and bandpass calibrators and 0238+166 for our phase calibrator. We calibrated the GMRT data manually using commands in CASA, with 6 rounds of phase-only self-calibration and 2 rounds of amplitude and phase self-calibration.

The radio light curve from the VLA is shown in Figure 7. The radio counterpart was very luminous at the time of our first observation, with a 10 GHz (rest-frame 12 GHz) luminosity of 10^{30} erg s $^{-1}$ Hz $^{-1}$. This high luminosity and fast variability timescale of the 10 GHz light curve implies a high brightness temperature and therefore we conclude that the emission is synchrotron radiation. In the first epoch, the 10 GHz observation had an in-band spectral index of $\alpha = -0.16 \pm 0.05$ where $F_\nu \propto \nu^{-\alpha}$. This is inconsistent with being in the optically

Table 4. Host galaxy properties (metallicities, mainly) from PyMCZ. (SFR is not from PyMCZ).

SFR	6.47 ± 1.3
E(B-V)	$0.220^{+0.023}_{-0.022}$
logR23	$0.903^{+0.012}_{-0.012}$
D02	$8.253^{+0.130}_{-0.128}$
Z94	$8.450^{+0.016}_{-0.010}$
M91	$8.219^{+0.026}_{-0.026}$
PP04_N2Ha	$8.200^{+0.010}_{-0.010}$
PP04_O3N2	$8.187^{+0.008}_{-0.009}$
P10_ONS	$8.708^{+0.024}_{-0.024}$
P10_ON	$8.172^{+0.046}_{-0.047}$
M08_N2Ha	$8.361^{+0.020}_{-0.021}$
M08_O3O2	$8.521^{+0.011}_{-0.011}$
M13_O3N2	$8.174^{+0.009}_{-0.009}$
M13_N2	$8.194^{+0.041}_{-0.042}$
KD02_N2O2	$7.567^{+0.722}_{-0.074}$
KK04_N2Ha	$8.381^{+0.028}_{-0.029}$
KK04_R23	$8.390^{+0.021}_{-0.021}$
KD02comb	$8.304^{+0.024}_{-0.024}$

Table 5. Properties of the host galaxy of ZTF18abvkwla. The stellar mass, star-formation rate, maximum age, and extinction are from a fit to the galaxy SED; the χ^2 refers to that fit. The metallicity [O/H] was measured using the host galaxy spectrum and is provided on the Z94 scale. This value corresponds to $0.6\times$ solar.

Stellar mass	M	$5.1^{+3.4}_{-2.0} \times 10^8 M_\odot$
Star-formation rate	SFR	$6.8^{+3.7}_{-4.6} M_\odot \text{ yr}^{-1}$
Maximum age	age	$7.5^{+30}_{-4.5} \times 10^7 \text{ yr}$
Extinction	Av	$0.72^{+0.17}_{-0.54} \text{ mag}$
	χ^2/dof	1.6 / 2
Metallicity	$12+\log[\text{O}/\text{H}]$	8.5

thick ($\alpha = -2.5$) or the optically thin ($\alpha = +0.7$) regimes of a spectrum arising from synchrotron self-absorption, which suggests that the peak of the SED is near 10 GHz at this epoch.

To avoid a large departure from the minimum-energy state, the brightness temperature T_B cannot exceed the equipartition temperature $T_{\text{eq}} \approx 10^{11}$ K (Readhead 1994) where

$$T_B = \frac{c^2}{2k_B v^2} \frac{f_\nu}{\pi \Theta^2} \quad (1)$$

and c is the speed of light, k_B is Boltzmann’s constant, v is the frequency of observation, f_ν is flux density, and

Table 6. Radio observations of ZTF18abvkwla. Upper limits are given as three times the image RMS. Bandwidth is 4 GHz at X-band (10 GHz), 4 GHz at C-band (6 GHz), 2 GHz at S-band (3 GHz), and 1 GHz at L-band (1.5 GHz).

Δt days	Facility	Obs. Date (UT)	Config.	ν (GHz)	Flux Density (mJy)
81	VLA	2018-12-01	C	10	0.364 ± 0.006
310	VLA	2019-07-19	BnA	10	0.061 ± 0.003
343	VLA	2019-08-21	A	6	0.089 ± 0.003
346	VLA	2019-08-24	A	3	0.067 ± 0.005
351	VLA	2019-08-29	A	1.5	0.135 ± 0.007
352	VLA	2019-08-30	A	10	0.045 ± 0.003
396	VLA	2019-10-13	A	10	0.031 ± 0.003
397	VLA	2019-10-14	A	6	0.033 ± 0.003
364	GMRT	2019-09-11	-	0.6	0.21 ± 0.05

Θ is the angular radius of the source. For a given flux density and observing frequency, the angular radius of the source is therefore

$$\Theta \gtrsim 2.1 \left(\frac{f_\nu}{\mu\text{Jy}} \right)^{1/2} \left(\frac{\nu}{\text{GHz}} \right)^{-1} \mu\text{as}. \quad (2)$$

Using our first X-band (10 GHz) observation, we find $\Theta \gtrsim 4.0 \mu\text{as}$ at $\Delta t = 81$ d. Using our L-band (1.5 GHz) observation, we find $\Theta \gtrsim 16 \mu\text{as}$ at $\Delta t = 351$ d. We can use the known distance of ZTF18abvkwla to convert the radius to a velocity, assuming constant-velocity expansion:

$$\Theta = \frac{\Gamma \beta c t}{2d_A(1+z)} \quad (3)$$

where Γ is the Lorentz factor, c is the speed of light, t is the time since explosion in the observer frame, d_A is the angular-diameter distance, and z is the source redshift. For ZTF18abvkwla, we find $\Gamma\beta > 0.66$ or $v > 0.55c$ at $\Delta t = 81$ d and $\Gamma\beta > 0.57$ or $v > 0.50c$ at $\Delta t = 351$ d.

Finally, we estimate the radio emission from the host galaxy. From Murphy et al. (2011), the predicted 1.4 GHz luminosity for a given star-formation rate is

$$\left(\frac{L_{1.4\text{GHz}}}{\text{erg s}^{-1} \text{ Hz}^{-1}} \right) \approx 1.57 \times 10^{28} \left(\frac{\text{SFR}_{\text{radio}}}{M_\odot \text{ yr}^{-1}} \right) \approx 10^{29} \text{ erg s}^{-1} \text{ Hz}^{-1}. \quad (4)$$

This luminosity corresponds to 0.04 mJy at the distance of ZTF18abvkwla, so the contribution of the host galaxy could be significant in the final epoch of our VLA observations. At 10 GHz (assuming a spectral index of -0.8 ; Condon 1992) the expectation is 0.01 mJy. Thus, the host galaxy is not a significant contribution to our X-band observations of ZTF18abvkwla.

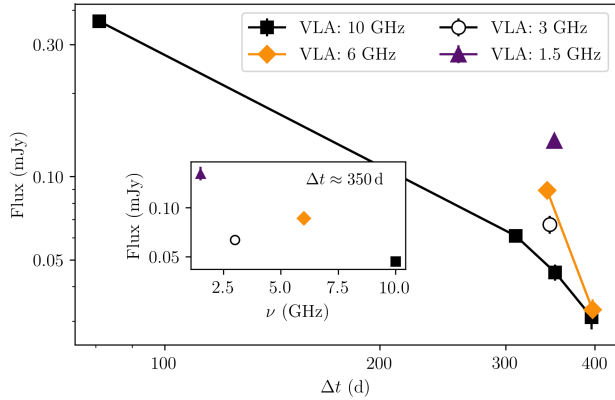


Figure 7. The radio light curves of ZTF18abvkwla with the spectral energy distribution at $\Delta t \approx 350$ d shown inset

3. COMPARISON WITH EXTRAGALACTIC EXPLOSIONS

3.1. Optical Light Curve and Spectrum

As discussed in Section 1, the fast rise time and high peak luminosity of ZTF18abvkwla are shared by only a handful of transients in the literature. Here we compare ZTF18abvkwla to iPTF15ul (Hosseinzadeh et al. 2017), DES16X1eho (Pursiainen et al. 2018), iPTF16asu (Whitesides et al. 2017; Wang et al. 2019), and AT2018cow (Prentice et al. 2018; Perley et al. 2019a). We exclude Dougie because it resided in an old stellar population with no signs of enhanced star formation (Vinkó et al. 2015); the dominance of absorption features and much lower star-formation rate were confirmed by additional LRIS spectroscopy (Arcavi et al. 2016).

For each transient, we selected the light curve in a filter closest to rest-frame g (the same filters used in constructing Figure 1). Following Whitesides et al. (2017), we corrected absolute magnitudes for redshift using the following equation

$$M = m_{\text{obs}} - 5 \log_{10} \left(\frac{D_L}{10 \text{ pc}} \right) + 2.5 \log_{10}(1+z). \quad (5)$$

We cannot perform a true K -correction because most objects lack sufficient spectroscopic coverage. These equations will introduce systematic errors on the order of 0.1 mag.

In Figure 8 we show the rest-frame g -band light curve of ZTF18abvkwla compared to the light curves of optical transients in Table 1. The fast rise time of ZTF18abvkwla is most similar to iPTF15ul, AT2018cow, and perhaps iPTF16asu. However, the fade time is much faster than that of iPTF16asu (which spectroscopically evolved into a Ic-BL SN) and is more sim-

ilar to that of iPTF15ul and AT2018cow. However, we caution that the high peak luminosity of iPTF15ul results from a large host-galaxy extinction inferred in Hosseinzadeh et al. (2017), without which the peak magnitude would be -19.6 and not included in this sample.

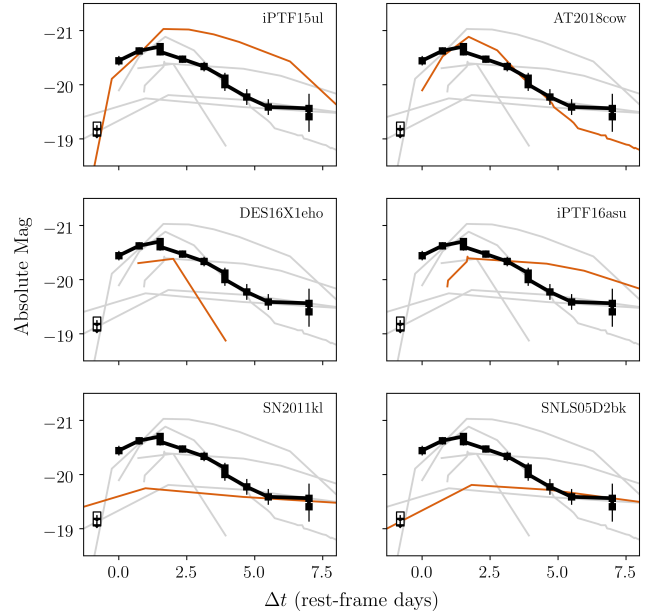


Figure 8. The rest-frame g -band (observer-frame r -band) light curve of ZTF18abvkwla (black line), compared to light curves of other transients in the literature in as close to the same rest-frame filter as possible. Each panel shows one transient highlighted in orange for comparison, with the rest shown in grey in the background.

Next we consider color evolution. ZTF18abvkwla showed tentative evidence for reddening over time, from $g - r = -0.47 \pm 0.09$ at peak to $g - r = -0.03 \pm 0.21$ in the final epoch a week later; however, this is only a $2\text{-}\sigma$ change. AT2018cow, iPTF15ul, and DES16X1eho remained very blue throughout the evolution of their optical light curves, whereas iPTF16asu reddened significantly as the SN became the dominant component.

Optical spectra were obtained for all events at peak light except for DES16X1eho. No features were detected in the peak spectra of iPTF16asu and AT2018cow, and iPTF15ul had a weak emission feature attributed to C III (Hosseinzadeh et al. 2017).

iPTF16asu developed features of a Ic-BL SN (Whitesides et al. 2017), and AT2018cow had a complex spectral evolution, with a broad feature ($\nu > 0.1c$) that appeared and disappeared over several days following peak light and emission lines one week later (Perley et al. 2019a). Like AT2018cow and iPTF16asu, no features are discernible in the peak-light spectrum of ZTF18abvkwla, and unfortunately we lack spectra dur-

ing the decline of the optical light curve. No spectra were obtained of DES16X1eho during outburst.

3.2. Radio Light Curve

In the previous section (Section 3.1), we compared the optical properties of ZTF18abvkwla to the transients in Table 1: the light curve shape, the color evolution, and the spectrum. In this section we compare the radio properties of ZTF18abvkwla to the same set of transients.

Figure 9 shows the 10 GHz light curve of ZTF18abvkwla (12 GHz rest-frame) to a variety of energetic transients in the literature. The sources at $\nu L_\nu < 10^{37} \text{ erg s}^{-1}$ are ordinary core-collapse SNe observed nearby, such as SN 1979C (Weiler et al. 1986) and SN 1993J (Weiler et al. 2007). The sources at intermediate luminosities ($10^{37} \text{ erg s}^{-1}$ to $10^{39} \text{ erg s}^{-1}$) include relativistic Ic-BL SNe like SN 2009bb (Soderberg et al. 2010) and SN 1998bw (Kulkarni et al. 1998), Ic-BL SNe with strong CSM interaction and a mildly relativistic outflow (e.g. SN 2003L; Soderberg et al. 2005), the TDE ASASSN14li (Alexander et al. 2016), and AT2018cow (Margutti et al. 2019). ZTF18abvkwla resides with the highest-luminosity events ($\nu L_\nu > 10^{39} \text{ erg s}^{-1}$): long-duration GRB afterglows (Berger et al. 2003; Perley et al. 2014) and a relativistic TDE (Zauderer et al. 2011; Berger et al. 2012).

As shown in Figure 9, the luminosity and steep decay of ZTF18abvkwla is most similar to that of GRB afterglows, particularly that of GRB 030329 (Berger et al. 2003). At 67 days post-explosion, the SED of GRB 030329 peaked around 5 GHz (Berger et al. 2003). At a similar epoch post-explosion, the SED of GRB 130427A peaked around 10 GHz (Perley et al. 2013). Thus, the SED of ZTF18abvkwla at $\Delta t = 81 \text{ d}$ is similar to that of GRBs at similar epochs.

Of the transients in Table 1, only AT2018cow had a detected radio counterpart. Prompt radio follow-up observations were obtained for iPTF15ul and iPTF16asu. Observations of iPTF15ul were obtained within five days of the optical discovery, two observer-frame days after peak optical light, at 6 GHz and 22 GHz with the VLA, at 15 GHz with the Arcminute Microkelvin Imager (Zwart et al. 2008), and at 95 GHz with the Combined Array for Research in Millimeter-wave Astronomy (Bock et al. 2006). There was no detection at any frequency, with an RMS of 0.235 mJy with CARMA and an RMS of 0.03 mJy with AML. The 6 GHz upper limit of three times the image RMS ($12 \mu\text{Jy}$) is shown in Figure 9. The limit rules out a normal GRB afterglow, and probably radio emission like that in SN 2009bb and SN 1998bw. However, since only one epoch was obtained and it was close to explosion, we cannot rule out a ris-

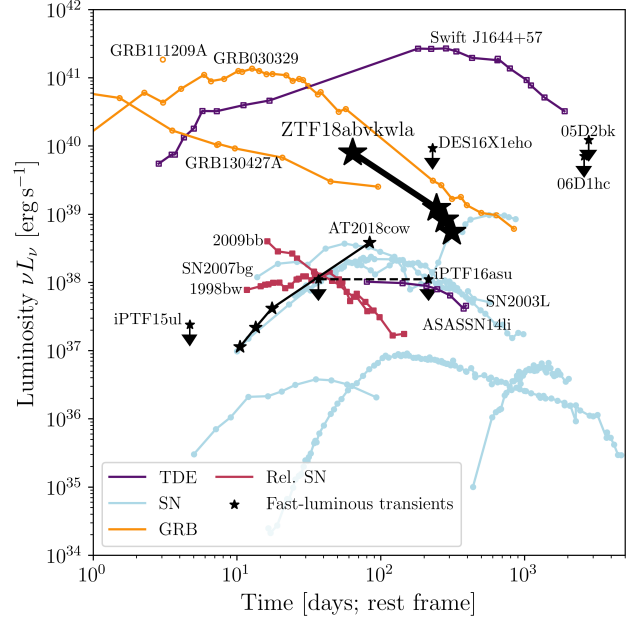


Figure 9. The 10 GHz radio light curve of ZTF18abvkwla compared to low-frequency (1–10 GHz) light curves of different classes of energetic explosions: tidal disruption events (TDEs; purple), supernovae exploding in dense CSM (blue lines, $\geq 10^{37} \text{ erg sec}$, relativistic Ic-BL supernovae (red lines), AT2018cow (black line, small stars), long-duration gamma-ray bursts (orange lines), and “ordinary” supernovae ($\leq 10^{37} \text{ erg s}^{-1}$). Light curves taken from Kulkarni et al. (1998), Stratta et al. (2013), Perley et al. (2014), Berger et al. (2003), van der Horst et al. (2014), Soderberg et al. (2010), Weiler et al. (1986), Weiler et al. (2007), Soderberg et al. (2004), Soderberg et al. (2005), Salas et al. (2013), Horesh et al. (2013), Krauss et al. (2012), and Margutti et al. (2019).

ing light curve like that seen in AT2018cow. Two radio observations of iPTF16asu also resulted in upper limits, shown at the center of the figure connected by a dashed line. These limits do rule out radio emission like that seen in AT2018cow and ZTF18abvkwla.

To our knowledge, Dougie, the SNLS transients, and DES16X1eho did not have prompt radio follow-up observations. However, the positions of DES16X1eho, 05D2bk, and 06d1hc were serendipitously covered by the VLA Sky Survey (VLASS; Lacy et al. 2019). VLASS has been mapping the entire sky visible to the VLA at low frequencies (2–4 GHz) in three epochs at a cadence of 32 months. The Quicklook images are now available for the first epoch ($17,000 \text{ deg}^{-2}$). We searched the existing Quicklook data using code available on Github² that locates the appropriate VLASS tile and subtile for a given RA and Dec and extracts a cutout 12 arcsec on a side.

² https://github.com/annayqho/Query_VLASS

Given a non-detection we estimated an upper limit on the flux density by taking the standard deviation of the pixel values in this cutout, after performing initial $3\text{-}\sigma$ clipping (removing pixels with a value greater than $3\times$ the standard deviation). None of these transients were detected, and we show the upper limits in Figure 9. Unfortunately these limits are too shallow even to rule out a GRB afterglow.

For completeness, we also searched the positions of all of the transients in the two largest collections of unclassified fast-rising luminous optical transients reported to date, PS1 (Drout et al. 2014) and the Dark Energy Survey (Pursiainen et al. 2018). None were detected, and the limits are listed in Table 7.

3.3. A Starburst Host Galaxy

In Sections 3.1 and 3 we compared the optical and radio properties of ZTF18abvkwla, respectively, to other transients in the literature. Here we put its host galaxy properties into context.

Starburst galaxies like the host of ZTF18abvkwla contribute a small fraction of star-formation in the low-redshift Universe (Lee et al. 2009). However, their contribution to low-metallicity star-formation is more significant, as they are typically low-mass and therefore low-metallicity (Tremonti et al. 2004). They are also promising candidates to experience a top-heavy IMF (Dabringhausen et al. 2009) and potential sites of enhanced binary or dynamical stellar interactions (van den Heuvel & Portegies Zwart 2013). Each of these mechanisms have been appealed to in attempts to interpret the relatively high abundance of exotic transients of other types found in these systems, including superluminous SNe (SLSNe; Quimby et al. 2011; Gal-Yam 2019), broad-lined Ic SNe (Modjaz et al. 2019), GRBs (Fruchter et al. 2006; Perley et al. 2013; Vergani et al. 2015), and at least some fast radio bursts (Katz 2016; Tendulkar et al. 2017).

Based on our measurements in Section 2.1.2 we conclude the following about the host of ZTF18abvkwla:

The host is not an AGN — We confirm the lack of any evidence for an optical AGN based on the very weak [NII] emission. The host falls squarely in the star-forming locus of the BPT diagram (Figure 10a).

The host metallicity is typical for its mass — The host is relatively metal-poor: the precise number is of course scale-dependent, but using the Z94 scale we calculate $[\text{O}/\text{H}]$ of 8.45, or about $0.6\times$ Solar. This is lower metallicity than the majority of star-formation in the local Universe, but not an outlier and unexceptional for low-mass galaxies in particular (Figure 10b).

Table 7. Radio limits for the subset of rapidly evolving transients in Drout et al. (2014) and Pursiainen et al. (2018) that have a subsequent VLASS observation. The Δt is the number of days between the discovery date as listed in Drout et al. (2014) or the time of peak as listed in Pursiainen et al. (2018) and the epoch of the VLASS observation of that field.

ID	RA [hh:mm:ss]	Dec [dd:mm:ss]	Δt (days)	Limit (μJy)
1-10ah	10:48:15.784	+57:24:19.48	2836	102
PS1-11qr	09:56:41.767	+01:53:38.25	2467	130
PS1-12bb	09:57:23.866	+03:11:04.47	2174	149
PS1-12brf	22:16:06.892	-00:58:09.81	1892	124
PS1-13duy	22:21:47.929	-00:14:34.94	1505	127
PS1-13dwm	22:20:12.081	+00:56:22.35	1422	155
PS1-10iu	16:11:34.886	+55:08:47.91	2689	103
PS1-13bit	16:12:00.765	+54:16:08.16	1618	104
PS1-13cgt	16:18:56.245	+54:19:33.71	1552	123
DES15S1fii	02:52:45.15	-00:53:10.21	826	150
DES13X3gms	02:23:12.27	-04:29:38.35	1520	139
DES15S1fil	02:51:09.36	-00:11:48.71	826	139
DES14S2anq	02:45:06.67	-00:44:42.77	1199	118
DES14X3pkl	02:28:50.64	-04:48:26.44	1100	105
DES15C3lpq	03:30:50.89	-28:36:47.08	849	145
DES16S1dxu	02:50:43.53	-00:42:33.29	385	154
DES15C3mgq	03:31:04.56	-28:12:31.74	835	99
DES16X1eho	02:21:22.87	-04:31:32.64	365	152
DES16X3cex	02:27:19.32	-04:57:04.27	393	128
DES15C3lzm	03:28:41.86	-28:13:54.96	839	106
DES13C3bcok	03:32:06.47	-28:37:29.70	1513	98
DES15C3nat	03:31:32.44	-28:43:25.06	810	108
DES15C3opk	03:26:38.76	-28:20:50.12	777	125
DES15C3opp	03:26:57.53	-28:06:53.61	781	112
DES13X3npb	02:26:34.11	-04:08:01.96	1411	122
DES16C3axz	03:31:14.15	-28:40:00.25	523	100
DES16C3gin	03:31:03.06	-28:17:30.98	391	107
DES14X1bnh	02:14:59.79	-04:47:33.32	1172	145
DES16X3ega	02:28:23.71	-04:46:36.18	357	111
DES15C3mfu	03:28:36.08	-28:44:20.00	835	187
DES13C3abtt	03:30:28.91	-28:09:42.12	1513	107
DES15C3pbi	03:28:56.68	-28:00:07.98	772	182
DES15X3atd	02:23:21.64	-04:17:28.95	830	146
DES13C3nxi	03:27:51.22	-28:21:26.21	1559	75
DES13C3smn	03:27:53.08	-28:05:00.93	1564	124
DES13X3aakf	02:22:50.84	-04:41:57.01	1441	108
DES13X3afjd	02:28:00.31	-04:34:59.39	1411	123
DES13X3kgm	02:26:00.92	-04:51:59.29	1508	103
DES16S2fqu	02:47:05.94	-00:20:50.40	356	139
DES16X1ddm	02:15:18.88	-04:21:52.07	386	111
DES16X3ddi	02:21:45.39	-04:41:08.95	393	127
DES16X3erw	02:24:49.31	-04:30:51.45	357	117

The starburst intensity is similar to extreme SLSN and GRB hosts — The most striking nature of the host galaxy is its very high specific star-formation rate, which is evident in Figure 10c and 10d.

The host of AT2018cow was also a dwarf galaxy, although it was more massive than that of ZTF18abvkwla and not starbursting, with a mass and star-formation rate of $1.4 \times 10^9 M_\odot$ and $0.22 M_\odot \text{ yr}^{-1}$ respectively (Perley et al. 2019a). The host galaxy of DES16X1eho had a stellar mass $\log(M) = 9.96^{+0.14}_{-0.51}$ and a specific SFR of $\log(\text{sSFR}) = -9.25$ (Pursiainen et al. 2018). The host galaxy of iPTF16asu had a stellar mass $\log(M) = 4.6^{+2.0}_{-2.3} \times 10^8 M_\odot$, and an H α sSFR of $0.7 M_\odot \text{ yr}^{-1}$ (Whitesides et al. 2017).

4. INTERPRETATION

Even with the small number of events in the Table 1 menagerie, there seem to be several different progenitor systems involved.

iPTF16asu was spectroscopically classified as a Type Ic-BL SN, the SN type associated with GRBs (Cano et al. 2017). Since then, another fast-luminous transient was discovered that evolved into a Type Ic-BL, SN2018gep (Ho et al. 2019b). iPTF16asu and SN2018gep have established that some Ic-BL SNe have an optical light curve that is dominated by a luminous thermal component at peak. This component is likely due to shock breakout or shock-cooling emission from CSM (Ho et al. 2019b), the same mechanism used to explain fast-luminous transients such as KSN2015K (Rest et al. 2018) and PTF09uj (Ofek et al. 2010). In these Ic-BL SNe, this emission may be related to the activity of a jet (Nakar 2015), but no radio emission was detected in either SN that would confirm the presence of a collimated relativistic outflow.

AT2018cow clearly had very different behavior from iPTF16asu: most notably, it never developed SN absorption features, had hydrogen and helium in its environment, and its radio counterpart was an order of magnitude more luminous than the limits set for iPTF16asu and SN2018gep. However, regardless of the origin, its optical light curve may have been powered by a similar mechanism, i.e. shock breakout in a shell or shock-cooling emission from extended material. Here we assume that the light curve of ZTF18abvkwla is also powered by one of these mechanisms, and consider what that implies about its physical properties.

4.1. Modeling the Optical Light Curve

Shock breakout occurs when the photon diffusion time drops below the shock crossing time ($\tau < c/v_s$, where τ is the optical depth and v_s is the shock velocity). For normal stellar progenitors, this emission is primarily at X-ray and UV wavelengths and lasts for seconds to a fraction of an hour. In the wake of this shockwave, the outer stellar material is heated to high temperatures, and as

it cools it radiates on the timescale of a day (“cooling envelope” emission). See Waxman & Katz (2017) for a review.

Prior to core-collapse, massive stars undergo mass-loss via steady winds or eruptive episodes (Smith 2014). As a result, a star can be surrounded by dense, recently-expelled material at the time of explosion. If this material is optically thick, it increases the effective radius of the star and prolongs the light curve from shock breakout. If the light curve of ZTF18abvkwla arises from shock breakout in a shell, we can estimate the radius of this extended material (CSM) assuming a rise to peak bolometric luminosity $t_{\text{rise}} < 2$ d, a peak luminosity $L_{\text{bol}} > 10^{44} \text{ erg s}^{-1}$ and a shock velocity of 10^4 km s^{-1} ; this is typical for SNe and consistent with the limit on the shock speed we estimated in Section 2.1.2 from the photospheric radius at peak light. This shock speed is much slower than the velocity we inferred for the radio emission in Section 2.2, and we discuss the implications of this in Section 4.2. The rise timescale is

$$t_{\text{BO}} \sim R_{\text{CSM}}/v_s = (1.3 \text{ d}) \left(\frac{R_{\text{CSM}}}{10^{15} \text{ cm}} \right) \left(\frac{v_s}{10^4 \text{ km s}^{-1}} \right)^{-1} \quad (6)$$

For ZTF18abvkwla, we find $R_{\text{CSM}} < 1.5 \times 10^{15} \text{ cm}$.

We can also estimate the mass in the shell, assuming that the shock deposits half its kinetic energy $(1/2)\rho v_s^2$ and that this deposited energy is $E_{\text{BO}} \sim 4\pi R^2 dR e_s$ where the energy density reflects the amount of thermal energy in the layer. The luminosity scales as

$$L_{\text{BO}} \sim \frac{E_{\text{BO}}}{t_{\text{cross}}} \sim \frac{v_s^3}{4} \frac{dM}{dR} \\ = (2.2 \times 10^{45} \text{ erg s}^{-1}) \left(\frac{v_s}{10^4 \text{ km s}^{-1}} \right)^3 \left(\frac{dM}{M_\odot} \right) \left(\frac{dR}{10^{15} \text{ cm}} \right)^{-1}. \quad (7)$$

Assuming $dR \sim R$, we find $M_{\text{CSM}} < 0.07 M_\odot$. In this framework, the differences in the light curves of different objects corresponds to differences in the shell mass, shell radius, and shock velocity. The luminosity is most sensitive to the velocity, so it is possible that the transients in Table 1 are distinguished by fast velocities, which would naturally explain the inclusion of a Ic-BL SN. For a fixed shock velocity, a fast rise time corresponds to a small shell radius, which in turn requires a large shell mass to produce a high luminosity.

Another possibility is that the light curve is powered not by shock breakout in a shell, but by post-shock envelope-cooling emission. For example, this was the model invoked for iPTF16asu (Whitesides et al. 2017),

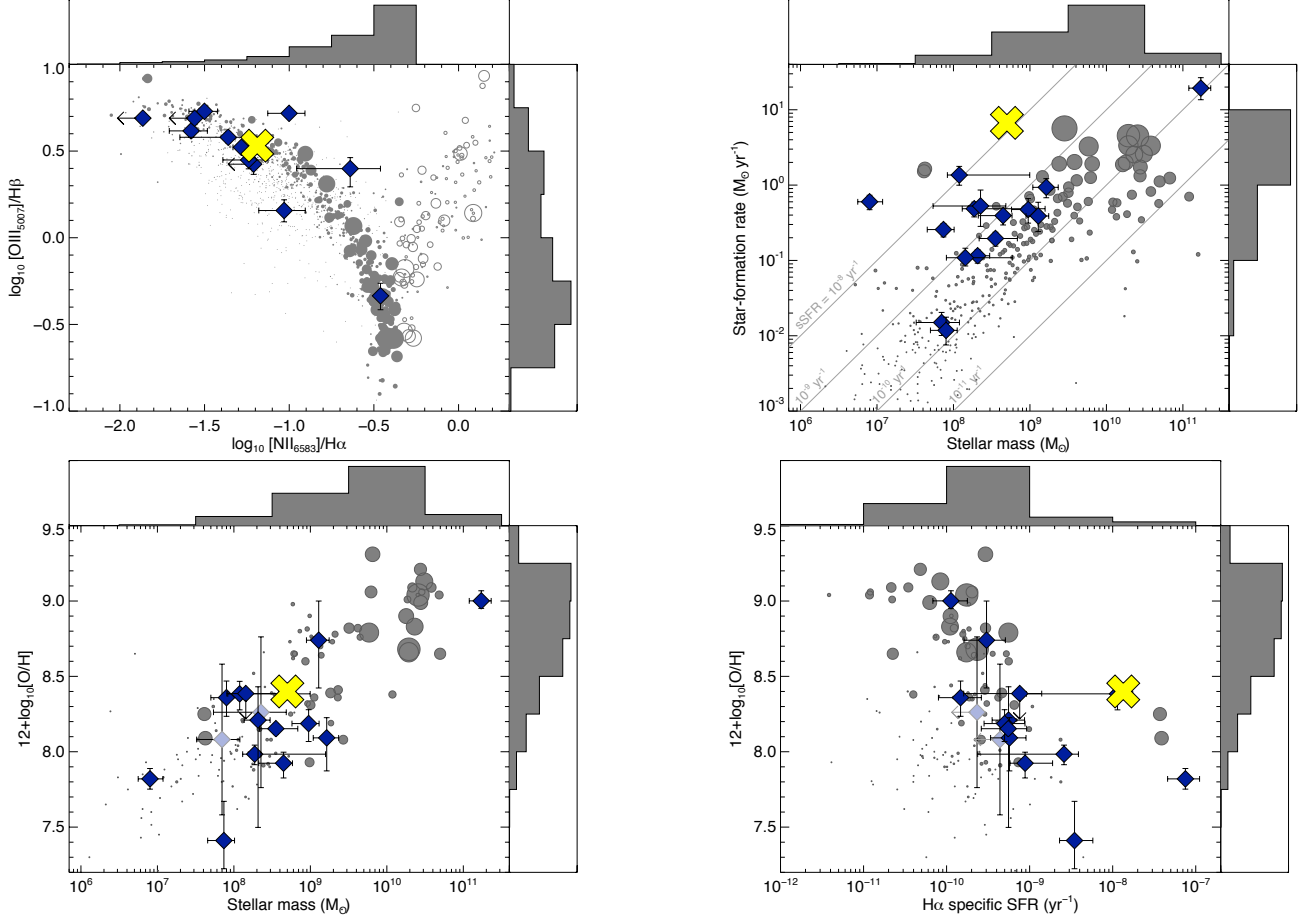


Figure 10. Comparison of the host galaxy of ZTF18abvkwla to <11 Mpc comparison galaxies (grey) and to nearby hydrogen-poor SLSNe (diamonds), as in Perley et al. 2016. Light diamonds indicate mass-metallicity estimated metallicities. Comparison galaxies are weighted by their SFR; histograms show the SFR-weighted binned totals on each axis. ZTF18abvkwla is indicated by a yellow cross. From top left: (a) BPT diagram. (b) Mass–star-formation rate relation. (c) Mass–metallicity relation. (d) Specific star-formation-rate–metallicity relation. The host is a starbursting galaxy with no evidence of AGN activity, and while it is metal-poor it is not particularly so given its mass.

which led to an inferred shell mass of $0.45 M_{\odot}$ and a shell radius of 1.7×10^{12} cm. The light curve of ZTF18abvkwla has a similar rise time but a higher peak luminosity than that of iPTF16asu, and the effective temperature at peak is significantly higher. According to the one-zone analytic formalism in Nakar, & Piro (2014) and Piro (2015), a higher peak temperature for a fixed rise time and a fixed opacity arises from a larger shell radius. A larger shell radius can also explain the higher bolometric luminosity, although that could also arise from a larger explosion energy or faster ejecta velocity.

Another mechanism suggested to explain the optical light curve of AT2018cow was reprocessing by dense outer ejecta (Margutti et al. 2019). In this picture, a central source (such as an accretion disk or magnetar) emits high-energy (i.e. X-ray) emission, which is reprocessed by surrounding material to produce lower-energy (i.e. optical) radiation. This is one setup for tidal disruption events, in which case the surrounding

material is unbound stellar debris (Strubbe & Quataert 2009). Indeed, several properties of ZTF18abvkwla and AT2018cow are similar to TDEs in the literature, such as the photospheric radius of 10^{14} – 10^{15} cm, the effective temperature of 10^4 K, and high radio luminosities attributed to jets (for reviews of TDE observations, see Gezari (2012) and Komossa (2015)).

Regardless of the power source at peak, we also use the optical light curve to put an upper limit on the mass of ^{56}Ni that could have been synthesized in the explosion. Using Equation (16) in Kasen (2017), the luminosity from the radioactive decay of ^{56}Ni is

$$L(t) = 2 \times 10^{43} \left(\frac{M_{\text{Ni}}}{M_{\odot}} \right) \times \left[3.9 e^{-t/\tau_{\text{Ni}}} + 0.678 \left(e^{-t/\tau_{\text{Co}}} - e^{-t/\tau_{\text{Ni}}} \right) \right] \text{erg s}^{-1} \quad (8)$$

where $\tau_{\text{Ni}} = 8.8 \text{ d}$ and $\tau_{\text{Co}} = 113.6 \text{ d}$. Using the r -band measurement at 8 days, $L \approx \lambda F_{\lambda} \approx 10^{43} \text{ erg s}^{-1}$, so the amount of ^{56}Ni that could power the light curve at this epoch is $M_{\text{Ni}} \lesssim 0.26 M_{\odot}$ (Figure 4). From a compilation of CC SNe, Lyman et al. (2016) found nickel masses of $0.11 \pm 0.04 M_{\odot}$ for Type IIb SNe, $0.17 \pm 0.16 M_{\odot}$ for Type Ib SNe, $0.22 \pm 0.16 M_{\odot}$ for Type Ic SNe, and $0.32 \pm 0.15 M_{\odot}$ for Type Ic-BL SNe. So, we cannot rule out any of these progenitors for ZTF18abvkwla.

4.2. Progenitor Systems and a Search for an Associated Gamma-ray Burst

The physical setups outlined in Section 4.1 — a shock driven through a shell, reprocessing of a high-energy compact source by optically thick material — could arise in a variety of different progenitor systems. An additional clue for ZTF18abvkwla is the host galaxy, which experienced a very recent burst of star-formation activity. In that sense, a massive-star origin seems most natural.

The photospheric velocity that we estimated in Section 2.1.2 was much smaller than the ejecta velocity we require for such luminous radio emission. As in AT2018cow, this suggests that the optical and radio emission come from two distinct components. The suggestion for AT2018cow was that a massive star collapsed and formed an accreting black hole. This engine drove a wide-angle fast ($v \sim 0.1c$) outflow, and a slower shock through dense equatorial material (Margutti et al. 2019). The fast outflow gave rise to the radio component, while the slower equatorial shock gave rise to the optical emission. A similar mechanism could be at work in ZTF18abvkwla, but with faster polar ejecta.

The luminous radio afterglow suggests that this could be a relative of GRBs, so we searched for potential gamma-ray burst counterparts to ZTF18abvkwla in the period between the last non-detection (MJD 58372.4206; 2018-09-11 10:05:39.84) and the first detection (MJD 58373.4075; 2018-09-12 09:46:48.00). There were two bursts detected by the interplanetary network (IPN; Hurley et al. 2010, 2016), one by the Gamma-ray Burst Monitor (GBM) aboard the *Fermi* spacecraft (Gruber et al. 2014; von Kienlin et al. 2014; Bhat et al. 2016) and one detected by the Konus-*Wind* experiment aboard the *Wind* spacecraft (Aptekar et al. 1995). The positions of both bursts are inconsistent with that of ZTF18abvkwla.

Due to the lack of detected GRB, we can set a limit on the fluence and corresponding isotropic equivalent energy of a prompt burst associated with ZTF18abvkwla. The IPN has essentially a 100% duty cycle across the sky, and detects GRBs with $E_p > 20 \text{ keV}$ down to $6 \times 10^{-7} \text{ erg cm}^{-2}$ at 50% efficiency (Hurley et al.

2010, 2016). At t_0 , the estimated 20–1500 keV limiting peak flux at the position of ZTF18abvkwla was $2 \times 10^{-7} \text{ erg cm}^{-2} \text{ s}^{-1}$ for a Band model that has E_{pk} in the 50–500 keV range. At the distance of ZTF18abvkwla, this corresponds to a limit on the isotropic peak luminosity of $L_{\text{iso}} < 5 \times 10^{49} \text{ erg s}^{-1}$. Therefore we strongly disfavor a classical GRB, but cannot rule out a lower-luminosity GRB (LLGRB) like those observed in conjunction with SN 2006aj and SN 1998bw (Cano et al. 2017).

As in the case of AT2018cow, we cannot rule out a TDE origin. In that case, the similarity to the light curve of AT2018cow would suggest a similar kind of system, i.e. an intermediate-mass black hole ($M \sim 10^4 M_{\odot}$; Perley et al. 2019a) with a white dwarf (Kuin et al. 2019) or a Solar-type (Perley et al. 2019a) stellar companion. In the case of AT2018cow, the main argument against a TDE hypothesis was the large ambient density (10^5 cm^{-3}) from millimeter (Ho et al. 2019a) and radio (Margutti et al. 2019) observations. For ZTF18abvkwla, assuming that the flat spectral index indicates a 10 GHz peak at 81 d, we find a much lower density (10^2 cm^{-3}). Among TDEs, the radio light curve of ZTF18abvkwla is most similar to that of the TDE candidate IGR J12580+0134 (Irwin et al. 2015), which had a nearly identical νL_{ν} (and fade rate) one year post-discovery. The radio emission from IGR J12580+0134 has been attributed to an off-axis relativistic jet (Irwin et al. 2015; Lei et al. 2016) but interpretation is complicated by the coincidence of the source with a known AGN.

5. RATE ESTIMATE

An important clue to the progenitor of sources like ZTF18abvkwla is the cosmological rate. Furthermore, three fast-luminous transients – SN 2011kl, AT2018cow, and ZTF18abvkwla – have detected luminous radio emission, so being able to recognize additional members of this phase-space in optical surveys would be valuable for radio follow-up observations. In this section, we conduct an archival search of 18 months of the 1DC survey (2018 Apr 3 – 2019 Oct 18 UT) to estimate the rate of transients in the phase-space of Figure 1 and delineate false positives.

First we selected field-nights in the survey for which the 1-night coverage was approximately maintained. Specifically, we require

- at least one observation the night before ($0.5 < dt < 1.5 \text{ days}$)
- at least one observation two nights before ($2.5 < dt < 1.5 \text{ days}$)

- at least three observations in the next five nights ($dt < 5.5$ days)

We find 8064 fields satisfying these criteria. Of these, 6854 fields (85%) have limiting magnitude > 19.75 mag and 4596 fields (57%) have limiting magnitude > 20.5 mag. The dominant effect is lunation, with some night-to-night variations due to weather.

For each of the 8064 field-nights, we searched for fast transients. To detect a fast transient, we require that the peak of the light curve be “resolved:” that is, that there are measurements both before and after peak light that are > 0.75 mag fainter than the peak magnitude. We then measure the time from 0.75 mag below peak to peak by linearly interpolating the light curve. If this rise time is < 5 d, we include the transient in our sample. More specifically, we filtered sources as summarized in Table 8. We scanned the remaining 659 sources by eye and removed sources with very noisy light curves or flaring behavior.

Table 8. Filtering criteria for sources similar to ZTF18abvkwla in the ZTF 1DC survey

Criteria	# sources remaining
Real ^a , bright ^b , pos. sub. ^c , not star ^d	758,528
Short duration ^e and peak resolved ^f	659

NOTE— ^a $drb > 0.99$ ^b $magpsf < 20$ ^c $isdiffpos='t'$ or $'1'$ ^d $not(sgscore1 > 0.76$ and $distpsnr1 < 1)$ ^e Duration between 1 and 100 days ^f Peak has preceding or subsequent detection/non-detection in a ± 5 d window that is at least 0.75 mag fainter

In Table 9 we list all 27 sources with rise times faster than 5 d, including ZTF18abvkwla itself. Five sources are spectroscopically classified SNe: two Type II, two Type Ibn, and one Type Iib. Three sources are classified as CVs, two spectroscopically and one by cross-matching with the AAVSO International Variable Star Index VSX (Watson et al. 2017). Two are very likely flare stars based on previous detections in Pan-STARRS individual-epoch images, and a third is a likely flare star based on a GALEX counterpart. Nine sources are likely extragalactic (based on proximity to a host galaxy). When redshift estimates for these galaxies were not available, we attempted to obtain them using LRIS on 17 Feb 2020. Two sources remain without definitive redshift estimates, so we provide a photometric redshift from LegacySurvey DR8. One source (ZTF18abxxeai) has a very faint host classified as a PSF in LegacySurvey DR8, and the remaining five sources have no clear host counterpart.

Of the sources with a definitive host redshift measurement, ZTF18abvkwla is the only one that is more luminous than $M = -20$. Clearly, the primary interlopers in

searches for transients like ZTF18abvkwla are CVs and less luminous SNe. CVs can be ruled out on the basis of repeated flaring, whereas less luminous SNe can only be ruled out if the redshift of the host galaxy is known *a priori*. Aside from ZTF18abvkwla, eight transients in our sample remain as possibly having $M_{g,peak} < -20$, although the lack of an obvious host for six of them suggest that these may be CVs.

We take eight as an upper limit for the number of transients in ZTF that could fall within the phase-space of Figure 1. Of these, three peak brighter than 19 mag, and four have a peak between 19 and 19.75 mag. We now calculate two all-sky rates. First we assume that the transient peaks at < 19 mag, in which case we discard field-nights with a limiting magnitude shallower than 19.75 mag. Then we assume that the transient peaks at < 19.75 mag, in which case we discard field-nights with a limiting magnitude shallower than 20.5 mag.

Each ZTF field is 47 deg^2 , but there is latitude-dependent overlap that has to be taken into account when converting this to a rate per square degrees in the sky. For the primary grid, a rough estimate of the fill factor is 87.5%. For the 1DC survey, the footprint is 10% smaller than the number of fields multiplied by 47 square degrees. So, taking fill factor and overlap into account, we estimate a typical area-per-field of 37 deg^2 . So for transients brighter than 19 mag we have $2.5 \times 10^5 \text{ deg}^2 \text{ d}$ and for transients brighter than 19.75 mag we have $1.7 \times 10^5 \text{ deg}^2 \text{ d}$. For transients peaking brighter than 19 mag we have a limiting all-sky rate

$$3 \times \frac{41253 \text{ deg}^2}{2.5 \times 10^5 \text{ deg}^2 \text{ d}} \times 365 \text{ d} \approx 180 \text{ yr}^{-1}. \quad (9)$$

For transients peaking brighter than 19.5 mag we have a limiting all-sky rate

$$4 \times \frac{41253 \text{ deg}^2}{1.7 \times 10^5 \text{ deg}^2 \text{ d}} \times 365 \text{ d} \approx 350 \text{ yr}^{-1}. \quad (10)$$

Now, we use the limiting magnitude to estimate a volumetric rate. Assuming a transient that peaks at $M = -20$, requiring a peak apparent magnitude brighter than 19 mag restricts our sensitivity to 400 Mpc. So, we find a volumetric rate of $7 \times 10^{-7} \text{ yr}^{-1} \text{ Mpc}^{-3}$. Requiring a peak apparent magnitude brighter than 19.75 mag restricts our sensitivity to 560 Mpc, leading to a volumetric rate of $4 \times 10^{-7} \text{ yr}^{-1} \text{ Mpc}^{-3}$. For reference, we provide rates of core-collapse SNe and GRBs in Table 10. The rate of events like ZTF18abvkwla appears to be two orders of magnitude smaller than the CC SN rate, and more similar to the rate of GRBs in the local universe.

6. PROSPECTS FOR DETECTING X-RAY EMISSION

Table 9. Fast-rising transients in ZTF resulting from our archival search of the one-day cadence survey. In the redshift column, a range refers to the 68 percentile range on the photometric redshift from LegacySurvey DR8 (we provide a corresponding range of absolute magnitude) and a single value corresponds to a spectroscopic redshift. When the distance is known, the peak mag is an absolute magnitude, and when the distance is not known the peak mag is an apparent magnitude. These values correspond to the filter as close to rest-frame g -band as possible, and when the distance is not known they correspond to the observed g -band filter. Magnitudes are corrected for Galactic extinction and timescales are in rest-frame when the redshift is known, and in observer-frame when the redshift is not known.

ZTF Name (IAU Name)	Redshift	Peak Mag	t_{rise}	t_{fade}	Type	Notes
18abvkwla	0.2714	-20.59 ± 0.07	1.83 ± 0.05	3.12 ± 0.22	Unknown	This paper
19aavbjfp (SN2019fkl)	0.028	-17.4 ± 0.4	3.2 ± 0.9	21.8 ± 6.1	SN II	
19abgbdcg (AT2019lbu)	0.0318	-18.36 ± 0.03	2.32 ± 0.03	14.4 ± 0.9	SN II	
18aalrxas	0.0588	-18.43 ± 0.03	1.86 ± 0.02	2.4 ± 0.3	SN I Ib	Fremling et al. (2019)
19abuvqgw (AT2019php)	0.087	-18.9 ± 0.1	3.6 ± 0.1	4.5 ± 0.3	SN Ibn	
19aapfmki (SN2019deh)	0.05469	-19.90 ± 0.01	4.38 ± 0.03	7.2 ± 0.4	SN Ibn	
18abskrix	Galactic	17.78 ± 0.02	1.26 ± 0.03	2.5 ± 0.2	CV	Spectroscopic classification
18absrffm (AT2018ftw)	Galactic	16.34 ± 0.01	2.60 ± 0.03	5.00 ± 0.03	CV	Spectroscopic classification
18abyzkeq	Galactic	18.32 ± 0.10	1.37 ± 0.04	0.93 ± 0.06	CV	AAVSO Name: CSS 151114:224934+375554
18ablxawt	Galactic	18.31 ± 0.04	2.4 ± 0.3	5.2 ± 0.9	Likely flare star	Previous detection in PS1 DR2 at $i = 19.4$
19abpwygn	-	16.74 ± 0.01	2.03 ± 0.03	1.73 ± 0.03	Likely flare star	Previous detection in PS1 DR2 at $z = 18.75$
18abyjgaa	-	18.39 ± 0.03	0.82 ± 0.03	2.05 ± 0.08	Likely flare star	GALEX source, possible flaring in PS1 DR2
18aasaiyp	0.104	-19.13 ± 0.05	1.9 ± 0.6	17.1 ± 0.6	Unknown	
18abuvqgo	0.155	-19.93 ± 0.05	4.7 ± 0.2	9.9 ± 0.6	Unknown	
18abydmfv (AT2018hkr)	0.042	-18.66 ± 0.03	3.15 ± 0.04	7.7 ± 2.5	Unknown	
18acepuyx (AT2018kxh)	0.0711	-19.1 ± 0.2	1.4 ± 0.3	10.8 ± 1.2	Unknown	
19aatoboa (AT2019esf)	0.0758	-18.90 ± 0.03	2.41 ± 0.03	4.9 ± 0.3	Unknown	
19abgbbpz (AT2019leo)	0.0625	-18.83 ± 0.03	4.2 ± 0.3	> 5	Unknown	
19abiyhd (AT2019lwj)	0.07	-18.11 ± 0.05	2.5 ± 0.2	4.1 ± 0.3	Unknown	
19aaadfcg	0.08–0.15	19.04 ± 0.04	2.44 ± 0.15	5.86 ± 0.15	Unknown	
19aanvhyc (AT2019coi)	0.056–0.076	18.41 ± 0.04	4.39 ± 0.04	12.1 ± 2.1	Unknown	‘PSF’ host in LegacySurvey DR8
18abxxeai	-	18.55 ± 0.06	1.9 ± 0.1	6.0 ± 0.8	Unknown	No clear host
18acgnwpo	-	18.90 ± 0.05	0.52 ± 0.03	6.5 ± 0.5	Unknown	No clear host
19aanqqzb	-	16.63 ± 0.04	1.91 ± 0.07	1.2 ± 0.1	Unknown	No clear host
19aaqfdvu	-	19.02 ± 0.06	2.0 ± 0.2	1.6 ± 0.4	Unknown	No clear host
19aaxfgyx	-	18.76 ± 0.03	0.98 ± 0.03	4.68 ± 0.27	Unknown	No clear host
19abzfzbs	-	19.36 ± 0.17	3.7 ± 2.2	13.4 ± 3.2	Unknown	No clear host

Clearly, radio observations are an important avenue of follow-up for transients like ZTF18abvkwla. Another valuable avenue is X-ray observations, which were not obtained for ZTF18abvkwla. We can estimate what the predicted X-ray luminosity would be from inverse Compton scattering, using the optical and radio luminosities:

$$\frac{L_X}{L_{\text{radio}}} = \frac{u_{ph}}{u_B}. \quad (11)$$

Taking $L_{\text{radio}} = 10^{40} \text{ erg s}^{-1}$, $u_{ph} = 10^{44} \text{ erg s}^{-1} / (4\pi R^3 / 3)$ where $R = 10^{14} \text{ cm}$, and $u_B = B^2 / 8\pi$ where $B = 0.6 \text{ G}$, we find $L_X \approx 10^{43} \text{ erg s}^{-1}$. This is even more luminous than the X-ray emission observed accompanying AT2018cow, which had $L_X \approx 10^{42} \text{ erg sec}$ (Rivera Sandoval et al. 2018; Ho et al. 2019a; Margutti et al. 2019). To our knowledge there were no X-ray follow-up observations of DES16X1eho, while observations of iPTF16asu resulted in an X-ray upper limit of $10^{43} \text{ erg s}^{-1}$. Hosseinzadeh et al. (2017) report pre-peak UV measurements from *Swift*

for iPTF15ul, but to our knowledge X-ray observations have not been reported. We measured an upper limit of $0.005 \text{ count s}^{-1}$ in a single epoch from the publicly available *Swift* data. Assuming $n_H = 1.7 \times 10^{20} \text{ cm}^{-2}$ and a power-law source model with a photon index $\Gamma = 2$ we obtain an upper limit on the unabsorbed 0.3–10 keV luminosity of $2 \times 10^{42} \text{ erg s}^{-1}$.

7. SUMMARY AND CONCLUSIONS

ZTF18abvkwla is distinguished by two key characteristics: a fast-evolving optical light curve with a hot ($T > 40,000 \text{ K}$) and featureless thermal spectrum at peak, and a long-lived, fast-fading radio light curve similar to those of jet-powered long-duration GRBs. The host galaxy underwent a recent starforming episode and has a very high specific star-formation rate, similar to that of extreme SLSN and GRB hosts. Events like ZTF18abvkwla are rare: from one year of the ZTF

Table 10. Local ($z = 0$) Rates of core-collapse supernovae and GRBs. Approximately 30% of CC SNe arise from a progenitor stripped of its hydrogen envelope. Among these stripped events, there are roughly equal numbers of IIb, Ib, and Ic events. Of the Ic events, $\sim 10\%$ are “broad-lined” with photospheric velocities $\gtrsim 30,000$ km/s. The fraction of Ic-BL SNe with associated GRBs has been constrained to $\lesssim 30\%$ (Corsi et al. 2016) although the rate is highly uncertain. The fraction of Ic-BL SNe with associated LLGRBs is roughly a factor of a few but also remains uncertain. Note that the rate quoted for LLGRBs does not include a beaming correction, so the “true” rate is probably a little higher, by a factor of a few. This is consistent with the relatively high detection fraction of radio emission from Ic-BL.

Class	Rate/Fraction	References
SN II	$4.47 \pm 1.39 \times 10^{-5} \text{ yr}^{-1} \text{ Mpc}^{-3}$	[1]
SN Ibc	$2.58 \pm 0.72 \times 10^{-5} \text{ yr}^{-1} \text{ Mpc}^{-3}$	[1]
Frac. of Ibc SN that are Ic	0.69 ± 0.09	[2,3]
Frac. of Ic SN that are Ic-BL	0.21 ± 0.05	[2,3]
LLGRB	$2.3^{+4.9}_{-1.9} \times 10^{-7} \text{ yr}^{-1} \text{ Mpc}^{-3}$	[4]
ℓ GRB	$\mathcal{R}_{\text{obs}} = 4.2^{+9.0}_{-4.0} \times 10^{-10} \text{ yr}^{-1} \text{ Mpc}^{-3}$	[5]
	$f_b = 0.0019 \pm 0.0003$	[6]
	$f_b = 0.013 \pm 0.004$	[7]

References—[1] Li et al. (2011), [2] Kelly & Kirshner (2012), [3] Graham & Schady (2016), [4] Soderberg et al. (2006), [5] Lien et al. (2014), [6] Frail et al. (2001), [7] Guetta et al. (2005)

IDC survey, we estimate that the rate is at least two orders of magnitude smaller than the CC SN rate.

Due to the lack of late-time photometry, we cannot conclude whether the late-time light curve was powered by the same mechanism as the peak or whether another mechanism such as nickel decay became dominant, and we have only tentative evidence for color evolution (cooling) over time. Furthermore, we cannot determine whether this source developed supernova features and whether it most closely resembles a Ic-BL like iPTF16asu, a continuum with emission lines like the Ibn iPTF15ul or the SN/TDE candidate AT2018cow, or neither.

Among the small group of sources with similar optical light curves, only AT2018cow had detected accompanying radio emission. Thus, AT2018cow and ZTF18abvkwla are the only two events in the literature established to have fast-blue optical light curves, likely powered by CSM interaction or reprocessing of high-energy emission, as well as a separate fast ejecta component that produces luminous radio emission. The component in ZTF18abvkwla appears to have been faster and more energetic than the component in AT2018cow.

Interestingly, most of the well-studied transients in Table 1 are associated with a candidate engine-powered explosion. AT2018cow had a long-lived central engine that powered a fast ($0.1c$) outflow. The Koala likely had a

central engine that powered an even faster ($> 0.5c$) outflow, perhaps a relativistic jet. iPTF16asu was a Ic-BL SN, and therefore by definition had faster ejecta velocities than ordinary core-collapse supernovae, although there was no evidence for a jet. SN 2011kl had a burst of high-energy emission and an associated luminous afterglow. Given the sensitivity of the luminosity to the shock speed (Equation 7), perhaps this apparent relationship between engine-driven supernovae and luminous fast-luminous optical transients should not be surprising.

At $z = 0.27$, ZTF18abvkwla was much more distant than AT2018cow ($z = 0.0141$), but the lesson from Section 2.2 and Section 5 is that we should not be deterred by cosmological distances in pursuing X-ray and radio follow-up observations. The radio emission from ZTF18abvkwla would be easily detectable by the VLA out to $z = 0.5$ (assuming $5 \mu\text{Jy}$ RMS in half an hour of integration time) or even out to $z = 0.8$ (when it would be $30 \mu\text{Jy}$). Assuming a *Swift*/XRT sensitivity limit of $4 \times 10^{-14} \text{ erg cm}^{-2} \text{ s}^{-1}$, the X-ray emission from ZTF18abvkwla may have been on the detection threshold. For a *Chandra* sensitivity limit an order of magnitude deeper, this may be on the detection threshold at $z = 0.7$. At these larger distances ($z = 0.5, z = 0.7$) the optical g -band magnitude would be 21.1 and 22.3 respectively. This is out of reach for current surveys like ZTF, but standard for LSST. The false positives in such a search are lower-luminosity explosions (Type IIb, II, and Ibn SNe) and CVs. These can be ruled out via knowledge of the host redshift (and therefore intrinsic luminosity), so we emphasize the need for extensive and reliable galaxy-redshift catalogs.

ACKNOWLEDGEMENTS

A.Y.Q.H. is supported by a National Science Foundation Graduate Research Fellowship under Grant No. DGE-1144469. This work was supported by the GROWTH project funded by the National Science Foundation under PIRE Grant No. 1545949. This research was funded in part by a grant from the Heising-Simons Foundation and a grant from the Gordon and Betty Moore Foundation through Grant GBMF5076, and benefited from interactions with Daniel Kasen and David Khatami also funded by that grant.

A.Y.Q.H. would like to thank the NRAO staff for their help with data calibration and imaging, particularly Steve Myers, Aaron Lawson, Drew Medlin, and Emmanuel Momjian. She is grateful for their support and hospitality her visit to Socorro when this work was performed. She thanks Gregg Hallinan and Brad Cenko for their advice on reducing the radio and X-ray data,

respectively, Jochen Greiner and Iair Arcavi for their assistance in obtaining the light curve of SN 2011kl, Miika Pursiainen for sharing light curves of DES fast-luminous transients, Jesper Sollerman for carefully reading the

manuscript, and Tony Piro and Ben Margalit for other helpful discussions. This work made use of the IPN master burst list (ssl.berkeley.edu/ipn3/masterli.html) maintained by Kevin Hurley.

APPENDIX

A. LIGHT-CURVE MEASUREMENTS

To construct Table 1, we used observed bands as close as possible to rest-frame g : g -band for $z < 0.15$, r -band for $0.15 < z < 0.45$, i -band for $0.45 < z < 0.78$, and z -band for $0.78 < z < 1.0$. We excluded transients with $z > 1.0$. We measured rise and fade times to 0.75 mag below peak by linearly interpolating the single-filter light curve, and measured uncertainties using a Monte Carlo with 1000 realizations of the light curve. Additional notes on each transient are below.

For iPTF15ul ($z = 0.066$; Hosseinzadeh et al. 2017) the uncertainty on the peak magnitude was dominated by the uncertainty from the host-galaxy extinction estimate. For AT2018cow ($z = 0.0141$; Prentice et al. 2018; Perley et al. 2019a) we used the time between the last non-detection and the first detection as an upper limit on the rise time, although we note that interpolation would give 0.4 d, much shorter than 3 d. We also corrected for 0.287 mag of Galactic extinction, which was not applied in Table 3 of Perley et al. (2019a). For a lower limit, we used the o -band detection before peak (dominated by r -band flux at this epoch), cor-

rected for 0.198 mag of Galactic extinction. We assumed $g - r = -0.4$ and $g - i = -0.7$.

For SN 2011kl ($z = 0.677$) we used column M_{4556} in Table 2 of Kann et al. (2019). These values are corrected for rest-frame extinction, and the contribution of the GRB afterglow and host galaxy. For SNLS04D4ec ($z = 0.593$), SNLS05D2bk ($z = 0.699$), and SNLS06D1hc ($z = 0.555$) we used the i -band light curve from Arcavi et al. (2016) and corrected for Milky Way extinction.

For Dougie ($z = 0.19$; Vinkó et al. 2015) we added an additional 0.1 mag in quadrature to account for the zero-point uncertainty, and corrected for 0.031 mag of Milky Way extinction. For iPTF16asu ($z = 0.187$; Whitesides et al. 2017) we could not measure the rise or peak magnitude in rest-frame g because observations in the appropriate filter (r) began only 3 days after peak. We estimated an upper limit to the peak magnitude by assuming that the $g - r$ color at peak was identical to the $g - r$ color during the first r -band measurement. We used the first r -band measurement as a lower limit. For the time from half-max to max, we used the observed g -band light curve instead. We obtained the i -band light curve of DES16X1eho ($z = 0.76$; Pursiainen et al. 2018) from M. Pursiainen (private communication).

REFERENCES

- Abolfathi, B., Aguado, D. S., Aguilar, G., et al. 2018, *ApJS*, 235, 42
- Alexander, K. D., Berger, E., Guillochon, J., Zauderer, B. A., & Williams, P. K. G. 2016, *ApJL*, 819, L25
- Aptekar, R. L., Frederiks, D. D., Golenetskii, S. V., et al. 1995, *SSRv*, 71, 265
- Arcavi, I., Wolf, W. M., Howell, D. A., et al. 2016, *ApJ*, 819, 35
- Bellm, E. C., & Sesar, B. 2016, *Astrophysics Source Code Library*, ascl:1602.002
- Bellm, E. C., Kulkarni, S. R., Graham, M. J., et al. 2019, *PASP*, 131, 018002
- Bellm, E. C., Kulkarni, S. R., Barlow, T., et al. 2019, *PASP*, 131, 068003
- Berger, E., Kulkarni, S. R., Pooley, G., et al. 2003, *Nature*, 426, 154
- Berger, E., Zauderer, A., Pooley, G. G., et al. 2012, *ApJ*, 748, 36
- Narayana Bhat, P., Meegan, C. A., von Kienlin, A., et al. 2016, *ApJS*, 223, 28
- Bianco, F. B., Modjaz, M., Oh, S. M., et al. 2016, *Astronomy and Computing*, 16, 54
- Bock, D. C.-J., Bolatto, A. D., Hawkins, D. W., et al. 2006, *Proc. SPIE*, 626713
- Bruzual, G., & Charlot, S. 2003, *MNRAS*, 344, 1000
- Campana, S., Mangano, V., Blustin, A. J., et al. 2006, *Nature*, 442, 1008
- Cano, Z., Wang, S.-Q., Dai, Z.-G., & Wu, X.-F. 2017, *Advances in Astronomy*, 2017, 8929054
- Cenko, S. B., Kulkarni, S. R., Horesh, A., et al. 2013, *ApJ*, 769, 130
- Cenko, S. B., Urban, A. L., Perley, D. A., et al. 2015, *ApJL*, 803, L24

- Chevalier, R. A. 1998, *ApJ*, 499, 810
- Chevalier, R. A., & Irwin, C. M. 2011, *ApJL*, 729, L6
- Condon, J. J. 1992, *ARA&A*, 30, 575
- Dabringhausen, J., Kroupa, P., & Baumgardt, H. 2009, *MNRAS*, 394, 1529
- De Colle, F., & Lu, W. 2019, arXiv e-prints, arXiv:1911.01442
- Dey, A., Schlegel, D. J., Lang, D., et al. 2019, *AJ*, 157, 168
- Drout, M. R., Chornock, R., Soderberg, A. M., et al. 2014, *ApJ*, 794, 23
- Duev, D. A., Mahabal, A., Masci, F. J., et al. 2019, *MNRAS*, 489, 3582
- Firth, R. E., Sullivan, M., Gal-Yam, A., et al. 2015, *MNRAS*, 446, 3895
- Fitzpatrick, E. L. 1999, *PASP*, 111, 63
- Fox, O. D., & Smith, N. 2019, *MNRAS*, 488, 3772
- Frail, D. A., Kulkarni, S. R., Sari, R., et al. 2001, *ApJL*, 562, L55
- Fremming, C., Ko, H., Dugas, A., et al. 2019, *ApJL*, 878, L5
- Fruchter, A. S., Levan, A. J., Strolger, L., et al. 2006, *Nature*, 441, 463
- Gal-Yam, A. 2019, *ARA&A*, 57, 305
- Gezari, S., Heckman, T., Cenko, S. B., et al. 2009, *ApJ*, 698, 1367
- Gezari, S. 2012, *European Physical Journal Web of Conferences*, 03001
- Giannios, D., & Metzger, B. D. 2011, *MNRAS*, 416, 2102
- Graham, J. F., & Schady, P. 2016, *ApJ*, 823, 154
- Graham, M. J., Kulkarni, S. R., Bellm, E. C., et al. 2019, *PASP*, 131, 078001
- Greiner, J., Mazzali, P. A., Kann, D. A., et al. 2015, *Nature*, 523, 189
- Gruber, D., Goldstein, A., Weller von Ahlefeld, V., et al. 2014, *ApJS*, 211, 12
- Guetta, D., Piran, T., & Waxman, E. 2005, *ApJ*, 619, 412
- Gupta Y., et al., 2017, *Current Science*, 113, 707
- Ho, A. Y. Q., Phinney, E. S., Ravi, V., et al. 2019, *ApJ*, 871, 73
- Ho, A. Y. Q., Goldstein, D. A., Schulze, S., et al. 2019, *ApJ*, 887, 169
- Högbom, J. A. 1974, *A&AS*, 15, 417
- Horesh, A., Stockdale, C., Fox, D. B., et al. 2013, *MNRAS*, 436, 1258
- Hosseinzadeh, G., Arcavi, I., Valenti, S., et al. 2017, *ApJ*, 836, 158
- Huang, K., Shimoda, J., Urata, Y., et al. 2019, *ApJL*, 878, L25
- Hurley, K., Golenetskii, S., Aptekar, R., et al. 2010, *American Institute of Physics Conference Series*, 330
- Hurley, K., Svinikin, D. S., Aptekar, R. L., et al. 2016, *ApJL*, 829, L12
- Irwin, J. A., Henriksen, R. N., Krause, M., et al. 2015, *ApJ*, 809, 172
- Kann, D. A., Klose, S., Zhang, B., et al. 2010, *ApJ*, 720, 1513
- Kann, D. A., Schady, P., Olivares E., F., et al. 2019, *A&A*, 624, A143
- Kasen, D. 2017, *Handbook of Supernovae*, ISBN 978-3-319-21845-8. Springer International Publishing AG, 2017, p. 939, 939
- Kasliwal, M. M., Kulkarni, S. R., Gal-Yam, A., et al. 2012, *ApJ*, 755, 161
- Kasliwal, M. M., Cannella, C., Bagdasaryan, A., et al. 2019, *PASP*, 131, 038003
- Katz, J. I. 2016, *Modern Physics Letters A*, 31, 1630013
- Kelly, P. L., & Kirshner, R. P. 2012, *ApJ*, 759, 107
- Komossa, S. 2015, *Journal of High Energy Astrophysics*, 7, 148
- Krauss, M. I., Soderberg, A. M., Chomiuk, L., et al. 2012, *ApJL*, 750, L40
- Kuin, N. P. M., Wu, K., Oates, S., et al. 2019, *MNRAS*, 487, 2505
- Kulkarni, S. R., Frail, D. A., Wieringa, M. H., et al. 1998, *Nature*, 395, 663
- Lacy, M., Baum, S. A., Chandler, C. J., et al. 2019, arXiv e-prints, arXiv:1907.01981
- Law, N. M., Kulkarni, S. R., Dekany, R. G., et al. 2009, *PASP*, 121, 1395
- Lee, J. C., Kennicutt, R. C., Funes, S. J. J. G., et al. 2009, *ApJ*, 692, 1305
- Lei, W.-H., Yuan, Q., Zhang, B., et al. 2016, *ApJ*, 816, 20
- Li, W., Chornock, R., Leaman, J., et al. 2011, *MNRAS*, 412, 1473
- Lien, A., Sakamoto, T., Gehrels, N., et al. 2014, *ApJ*, 783, 24
- Lu, W., & Bonnerot, C. 2020, *MNRAS*, 492, 686
- Lyman, J. D., Bersier, D., James, P. A., et al. 2016, *MNRAS*, 457, 328
- Lyutikov, M., & Toonen, S. 2019, *MNRAS*, 487, 5618
- Mahabal, A., Rebbapragada, U., Walters, R., et al. 2019, *PASP*, 131, 038002
- Margutti, R., Metzger, B. D., Chornock, R., et al. 2019, *ApJ*, 872, 18
- Masci, F. J., Laher, R. R., Rusholme, B., et al. 2019, *PASP*, 131, 018003
- Matheson, T., Filippenko, A. V., Chornock, R., et al. 2000, *AJ*, 119, 2303

- McMullin, J. P., Waters, B., Schiebel, D., Young, W., & Golap, K. 2007, *Astronomical Data Analysis Software and Systems XVI*, 376, 127
- Miller, A. A., Yao, Y., Bulla, M., et al. 2020, arXiv e-prints, arXiv:2001.00598
- Modjaz, M., Bianco, F. B., Siwek, M., et al. 2019, arXiv e-prints, arXiv:1901.00872
- Murphy, E. J., Condon, J. J., Schinnerer, E., et al. 2011, *ApJ*, 737, 67
- Nakar, E., & Piro, A. L. 2014, *ApJ*, 788, 193
- Nakar, E. 2015, *ApJ*, 807, 172
- Nakar, E., & Piran, T. 2017, *ApJ*, 834, 28
- Ofek, E. O., Rabinak, I., Neill, J. D., et al. 2010, *ApJ*, 724, 1396
- Oke, J. B., & Gunn, J. E. 1982, *PASP*, 94, 586
- Oke, J. B., & Gunn, J. E. 1983, *ApJ*, 266, 713
- Oke, J. B., Cohen, J. G., Carr, M., et al. 1995, *PASP*, 107, 375
- Patterson, M. T., Bellm, E. C., Rusholme, B., et al. 2019, *PASP*, 131, 018001
- Perley, R. A., Chandler, C. J., Butler, B. J., et al. 2011, *ApJL*, 739, L1
- Perley, D. A., Levan, A. J., Tanvir, N. R., et al. 2013, *ApJ*, 778, 128
- Perley, D. A., Cenko, S. B., Corsi, A., et al. 2014, *ApJ*, 781, 37
- Perley, D. A., Quimby, R. M., Yan, L., et al. 2016, *ApJ*, 830, 13
- Perley, D. A., Mazzali, P. A., Yan, L., et al. 2019, *MNRAS*, 484, 1031
- Perley, D. A. 2019, *PASP*, 131, 084503
- Pietka, M., Fender, R. P., & Keane, E. F. 2015, *MNRAS*, 446, 3687
- Piro, A. L. 2015, *ApJL*, 808, L51
- Planck Collaboration, Ade, P. A. R., Aghanim, N., et al. 2016, *A&A*, 594, A13
- Prentice, S. J., Maguire, K., Smartt, S. J., et al. 2018, *ApJL*, 865, L3
- Pursiainen, M., Childress, M., Smith, M., et al. 2018, *MNRAS*, 481, 894
- Quimby, R. M., Kulkarni, S. R., Kasliwal, M. M., et al. 2011, *Nature*, 474, 487
- Rau, A., Kulkarni, S. R., Law, N. M., et al. 2009, *PASP*, 121, 1334
- Readhead, A. C. S. 1994, *ApJ*, 426, 51
- Rest, A., Garnavich, P. M., Khatami, D., et al. 2018, *Nature Astronomy*, 2, 307
- Rivera Sandoval, L. E., Maccarone, T. J., Corsi, A., et al. 2018, *MNRAS*, 480, L146
- Salas, P., Bauer, F. E., Stockdale, C., & Prieto, J. L. 2013, *MNRAS*, 428, 1207
- Schlafly, E. F., & Finkbeiner, D. P. 2011, *ApJ*, 737, 103
- Scott, M. A., & Readhead, A. C. S. 1977, *MNRAS*, 180, 539
- Shivvers, I., Modjaz, M., Zheng, W., et al. 2017, *PASP*, 129, 054201
- Slysh, V. I. 1990, *Soviet Astronomy Letters*, 16, 339
- Smith, N., & McCray, R. 2007, *ApJL*, 671, L17
- Smith, N. 2014, *ARA&A*, 52, 487
- Soderberg, A. M., Kulkarni, S. R., Berger, E., et al. 2004, *Nature*, 430, 648
- Soderberg, A. M., Kulkarni, S. R., Berger, E., et al. 2005, *ApJ*, 621, 908
- Soderberg, A. M., Kulkarni, S. R., Nakar, E., et al. 2006, *Nature*, 442, 1014
- Soderberg, A. M., Chakraborti, S., Pignata, G., et al. 2010, *Nature*, 463, 513
- Stratta, G., Gendre, B., Atteia, J. L., et al. 2013, *ApJ*, 779, 66
- Strubbe, L. E., & Quataert, E. 2009, *MNRAS*, 400, 2070
- Swarup, G., Ananthakrishnan, S., Kapahi, V. K., et al. 1991, *Current Science*, 60, 95
- Tachibana, Y., & Miller, A. A. 2018, *PASP*, 130, 128001
- Taggart, K., & Perley, D. 2019, arXiv e-prints, arXiv:1911.09112
- Tendulkar, S. P., Bassa, C. G., Cordes, J. M., et al. 2017, *ApJL*, 834, L7
- Tremonti, C. A., Heckman, T. M., Kauffmann, G., et al. 2004, *ApJ*, 613, 898
- van den Heuvel, E. P. J., & Portegies Zwart, S. F. 2013, *ApJ*, 779, 114
- van der Horst, A. J., Paragi, Z., de Bruyn, A. G., et al. 2014, *MNRAS*, 444, 3151
- Vergani, S. D., Salvaterra, R., Japelj, J., et al. 2015, *A&A*, 581, A102
- Vinkó, J., Yuan, F., Quimby, R. M., et al. 2015, *ApJ*, 798, 12
- von Kienlin, A., Meegan, C. A., Paciesas, W. S., et al. 2014, *ApJS*, 211, 13
- Wang, L. J., Wang, X. F., Cano, Z., et al. 2019, *MNRAS*, 489, 1110
- Watson, C., Henden, A. A., & Price, A. 2017, *VizieR Online Data Catalog*, B/vsx
- Waxman, E., & Katz, B. 2017, *Handbook of Supernovae*, 967
- Weiler, K. W., Sramek, R. A., Panagia, N., van der Hulst, J. M., & Salvati, M. 1986, *ApJ*, 301, 790
- Weiler, K. W., van Dyk, S. D., Panagia, N., Sramek, R. A., & Discenna, J. L. 1991, *ApJ*, 380, 161

Weiler, K. W., Williams, C. L., Panagia, N., et al. 2007, ApJ, 671, 1959
Whitesides, L., Lunnan, R., Kasliwal, M. M., et al. 2017, ApJ, 851, 107
Yao, Y., Miller, A. A., Kulkarni, S. R., et al. 2019, arXiv e-prints, arXiv:1910.02967

Zackay, B., Ofek, E. O., & Gal-Yam, A. 2016, ApJ, 830, 27
Zauderer, B. A., Berger, E., Soderberg, A. M., et al. 2011, Nature, 476, 425
Zwart, J. T. L., Barker, R. W., Biddulph, P., et al. 2008, MNRAS, 391, 1545